ISET Journal of Earthquake Technology, Paper No. 439, Vol. 41, No. 1, March 2004, pp. 15-52

DISPLACEMENT MODELLING OF INTRAPLATE EARTHQUAKES

Nelson Lam and John Wilson
Department of Civil and Environmental Engineering
University of Melbourne
Parkville 3010, Australia

ABSTRACT

This paper presents the case for a displacement-based approach for the seismic design and performance assessment of structures in intraplate regions. A newly established model for predicting seismic displacement demand is introduced. The presented material is based on outcomes from research which integrates expertise in the fields of engineering seismology, soil dynamics, structural dynamics and structural engineering. The analysis of a theoretical fault-slip function predicts peak displacement demand (in millimeters) equal to 10^{M-5} at 30 km hypocentral distance in "hard rock" conditions, where *M* is the moment magnitude of the earthquake. Significantly, the theoretical predictions have been shown to be highly consistent with predictions by both stochastic and empirical models which were developed from recorded ground motions. The effects of crustal modifications, attenuation, and site amplification are taken into account by component factors. Expressions for each of these factors are summarised in the table at the end of the paper and illustrated with a worked example in Appendix A to facilitate their practical applications.

KEYWORDS: Displacement, Performance-Based Design, Intraplate Earthquakes, Component Attenuation Model

INTRODUCTION

Earthquake engineering research in high seismic countries such as United States, Japan and New Zealand for over three decades have resulted in the development of design and detailing methodologies, which ensure that structures can safely withstand severe ground shaking without sustaining excessive damage and casualties. These significant research achievements culminated in the publication of numerous well used text books (Park and Paulay, 1975; Paulay and Priestley, 1992) and review articles (e.g., Park, 1997), which present an established static force-based (FB) procedure for earthquake resistant design incorporating capacity principles. The FB procedure (Figure 1) is based on the notion that the seismically induced strength demand is a function of the elastic acceleration response spectrum defined at the initial elastic natural period. The ductility of the structure, once substantiated, allows the elastic force demand to be reduced in accordance with the inelastic design spectra (as if ductility capacity could be traded off with strength capacity). The use of inelastic response spectra to represent seismic demand has been the focus of research for over two decades as evidenced by the numerous models that have been developed worldwide (e.g., Anagnostopoulos et al., 1978; Lai and Biggs, 1980; Mahin and Lin, 1983; Miranda, 1993; Lam et al., 1998).

Significantly, certain fundamental assumptions in the procedure have been found to be contradictory with real structural behaviour (Priestley, 1993). For example, the effective stiffness of a cracked reinforced concrete member is not constant but was found to increase with increasing flexural strength, since the flexural displacement of a concrete beam, or column, at yield is mainly a function of the dimensions of the section rather than the yield strength (Priestley, 1998). Furthermore, the force-displacement behaviour of a cracked concrete column is sensitive to the level of axial compression and is highly non-linear even before incipient yield condition is reached. Consequently, the stiffness behaviour of reinforced concrete is much more complex than was assumed in traditional modelling approaches, even if the effects of tension stiffening and interaction of the structure with non-structural components have been included. Difficulties in generalizing structural stiffnesses in the design process result in significant inaccuracies in defining the natural period of the structure and the corresponding strength demand calculated from the FB procedure. Significantly, when structural drift is required to be checked in satisfying performance-based requirements, the stiffness values must be used twice in the calculations:

(i) for the determination of the natural period which is, in turn, required for the calculation of the quasi-static seismic forces, and (ii) for the determination of drifts based on the calculated earthquake forces. If the natural period is determined by simple code rules (typically expressed as a function of the building height), the stiffness implicitly assumed in the period formula could be inconsistent with the stiffness used in the drift calculation.

The assumptions associated with the definition of the seismic demand in the FB procedure also requires critical examination. The use of acceleration response spectrum in the procedure to define seismic design is based on the notion that earthquake ground shaking is best represented by an accelerogram. Traditionally, compatible accelerograms have been selected on the basis of a reasonable match to the acceleration response spectrum. It is now recognised that the correct selection of accelerograms and a proper filtering procedure are critical for capturing the displacement demand of an earthquake associated with the long period motion components.

Despite these modelling errors, structures designed in accordance with capacity design principles (Figure 1) would still perform satisfactorily because of their inherent ductility and displacement capacity. However, an alternative procedure with assumptions that are more consistent with both ground shaking behaviour and structural response behaviour is required for engineering design particularly in the very diverse intraplate regions where non-ductile construction is common.

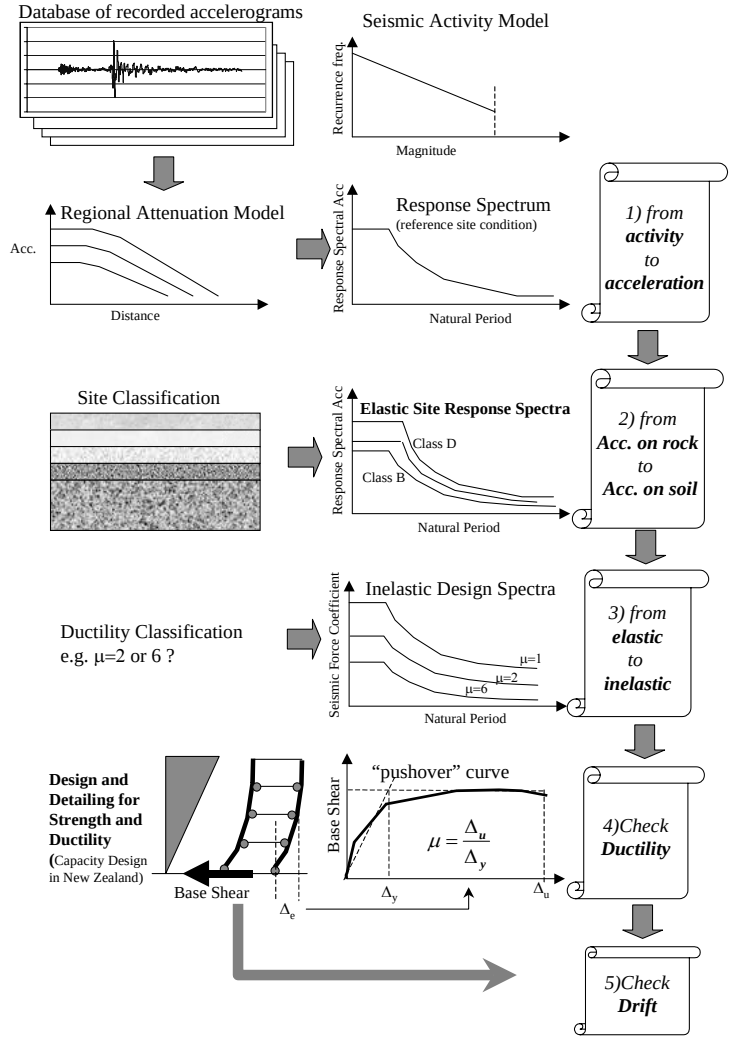

Fig. 1 Static force-based (FB) procedure

An innovative displacement-based (DB) procedure was proposed in recognition of the intrinsic deficiencies with the conventional FB procedure (Priestley, 1995, 2000; Priestley and Kowalsky, 2000). As shown in Figure 2, the DB procedure begins with equating the displacement demand to the displacement capacity of the structure. The need to calculate the displacement demand from a pre-

determined notional initial stiffness is therefore avoided. However, iterations are required in the DB procedure if equivalent damping is to be modelled with good precision. The displacement spectrum, which represents the seismic demand for the estimated level of damping, is then used in conjunction with the force-displacement relationship of the structure to calculate the strength demand. The incorporation of a realistic behaviour of the structure in the DB procedure makes the method transparent and versatile, which are essential qualities for the adaptation of the method to low to moderate intraplate seismic regions.

Intuitively, accelerograms recorded locally seem ideal for representing future earthquakes in an area, and in the absence of such records, accelerograms recorded from other intraplate regions such as Central and Eastern North America (CENA) appear as "second-best" alternatives. Such widely held notions are critically examined in the next section in which key mechanisms contributing to the frequency contents of earthquake ground shaking are considered in the context of intraplate earthquakes. In the displacement model, introduced in this paper, the displacement spectrum is not derived from the acceleration response spectrum (as has been done in regions of high seismicity with an abundance of recorded strong motion data), but is determined directly from given geophysical and geotechnical parameters. The key contribution of this paper is the introduction of a generic model for the prediction of seismic displacement demand, on both rock and soil sites, which is outlined in the third and fourth sections.

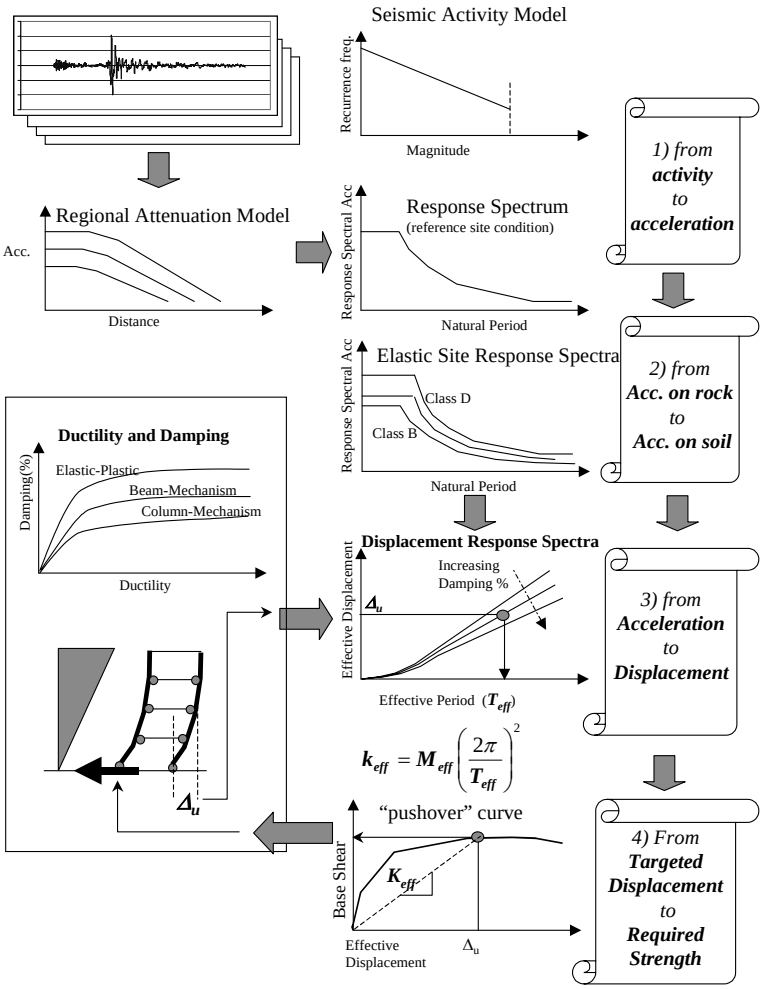

Fig. 2 Direct displacement-based (DB) procedure

The model will be illustrated in the fifth section of this paper using real case study examples in Australia. Some aspects of the displacement method have also been discussed by Kwong et al. (2000) in the context of potential applications in Hong Kong. The application of the DB procedure to the seismic assessment of unreinforced masonry walls is beyond the scope of this paper and has been discussed elsewhere (Doherty et al., 2002).

INTRAPLATE DISPLACEMENT MODEL IN PERSPECTIVE

The amplitude and frequency content of earthquake ground motion is a function of the magnitude (i.e. size) of the earthquake source, the type of faulting, the stress-drop behaviour, and the properties of the earth crust which could significantly modify seismic waves transmitted from the source of the earthquake to the ground surface. Crustal properties are regional dependent and must be distinguished from site properties which concern only the wave modification behaviour of the soil sediments overlying bedrock. An accelerogram recorded in the field contains information on the combined effects of all these component factors. Figures 3(a)-3(c) depict an earthquake accelerogram as a notional "bag" containing items of information each of which represents a component contribution to the earthquake ground motion. This component concept is central to the following discussion on modelling in intraplate regions where strong motion accelerogram records are generally lacking.

There are uncertainties as to whether small and large magnitude earthquakes can be represented by a single scaling relationship (Gibson et al., 1995). The uncertainties are due to possible change in the so called "stress-drop" behaviour which could influence the frequency content of the seismic waves radiating from the source of the earthquake. Thus, although a fair amount of instrumented data of earthquake tremors and small magnitude aftershocks may have been collected in a region, reliable attenuation relationships, which represent characteristics of potential large magnitude local earthquakes, cannot be developed solely from such data (refer Figure 3(a)).

Stress-drop behaviour also depends on the tectonic characteristics of the region. Consequently, it is unreliable to extrapolate observations from high seismic regions to low-moderate seismic regions even with similar earthquake magnitudes. Furthermore, the properties of the earth crust can also be very different between two regions. Problems associated with this inter-regional extrapolation is shown in Figure 3(b).

It should be noted that crustal properties could vary significantly within intraplate regions. For example, crustal conditions in Australia are highly variable even though the continent is wholly intraplate (Dowrick et al., 1995). This variability is reflected in different attenuation relationships that have been proposed for Western and Eastern Australia based on historical intensity data (Gaull et al., 1990). Thus, ground motion models developed from CENA cannot be automatically adapted to intraplate regions worldwide which are characterized by a diversity of crustal conditions (refer Figure 3(c)).

The authors have adopted a modeling approach based on resolving earthquake motions into individual component contributions (refer Lam and Wilson (2003) for an overview). For example, a generic intraplate source model could be developed if all intraplate earthquakes are assumed to possess a similar high level of stress drop and have reversed faulting mechanisms (refer Sub-section 1 in the next section). Meanwhile, the crustal properties of the region could be studied from local geophysical measurements in conjunction with existing geological information. The developed generic source model could then be combined with a representative regional model of the earth crust and the surface soil to produce a predictive ground motion model for the region (refer Figure 4).

This modelling methodology of resolving and re-assembling component contributions to earthquake ground motions is the basis of the Component Attenuation Model (CAM), the early form of which was introduced by the authors in Lam et al. (2000a, 2000b). The concept of decoupling the earthquake source and path effects is not new as this has been used in the development of the seismological models for the CENA region since the early 1980s (e.g., Boore, 1983). CAM, which predicts response spectrum parameters for direct engineering applications, is unique in that it has been developed to meet the engineering needs for an intraplate model that could be applied around the world. A robust relationship between the maximum displacement demand on the building and the moment magnitude of the earthquake has been identified for the generic "source" factor (refer Sub-section 1 in the next section). The incorporation of locally measured geophysical parameters in the modelling procedure to account for the "path" and "site" effects enables CAM to be used as a portable predictive tool (refer Sub-sections 2-3 in the next section). The emphasis on seismic displacement demand in CAM is consistent with performance-based engineering concepts.

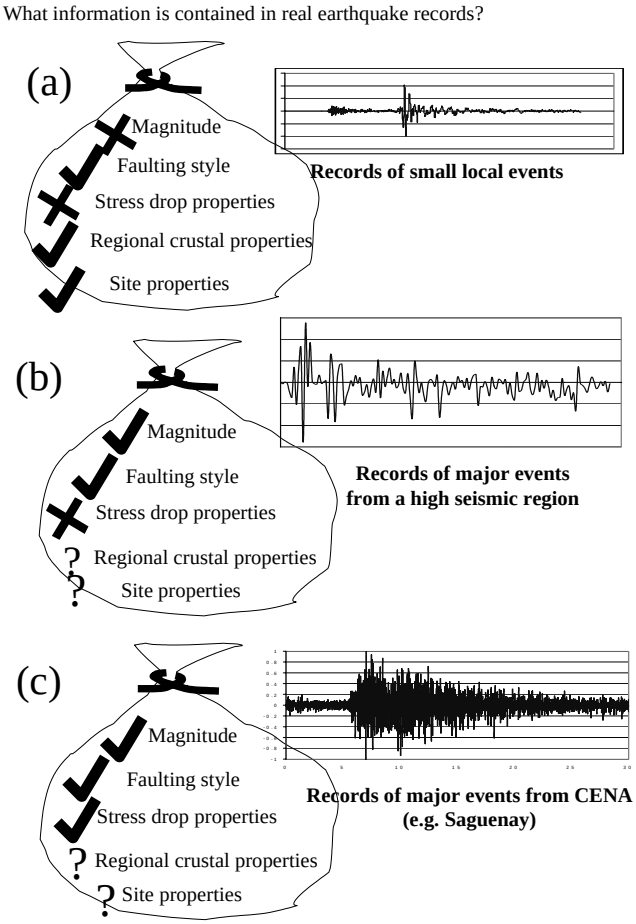

Fig. 3 Component contributions to intraplate earthquakes

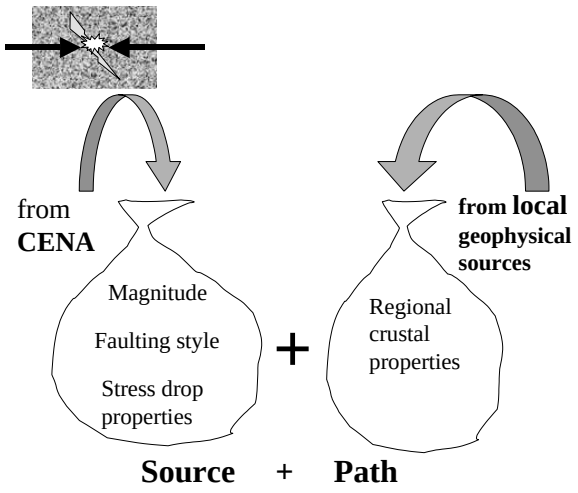

Fig. 4 Proposed modelling approach

CAM provides predictions for the following response spectrum parameters: $RSD_{\max}$, $RSV_{\max}$ and $RSA_{\max}$ which are the maximum values of the displacement, velocity and acceleration response spectrum respectively. The definitions for these parameters are shown in Figures 5(a)-5(d), which present response spectra in different formats, each having its own attributes. For example, the usual acceleration (RSA) format, adopted by traditional codes of practices, is suited to force-based seismic design procedures in which the acceleration demand is defined by the spectrum. The alternative velocity (RSV) format, plotted

on a logarithmic scale, could effectively present frequency contents over a broad frequency range of interests and hence is most suited for displaying, or comparing, the frequency properties of recorded earthquake motions. The capacity spectrum (ADRS) format, which has been used since the 1970s but has only recently been published (Freeman, 1998; ATC, 1996), is suited for comparing seismic demand curves with capacity (force-displacement) curves obtained from a pushover analysis of the structure. Amplification of the displacement demand is most conveniently represented by the displacement spectrum which is ideal for use in the direct displacement-based (DB) design or assessment procedure (Priestley, 1995, 2000; Priestley and Kowalsky, 2000).

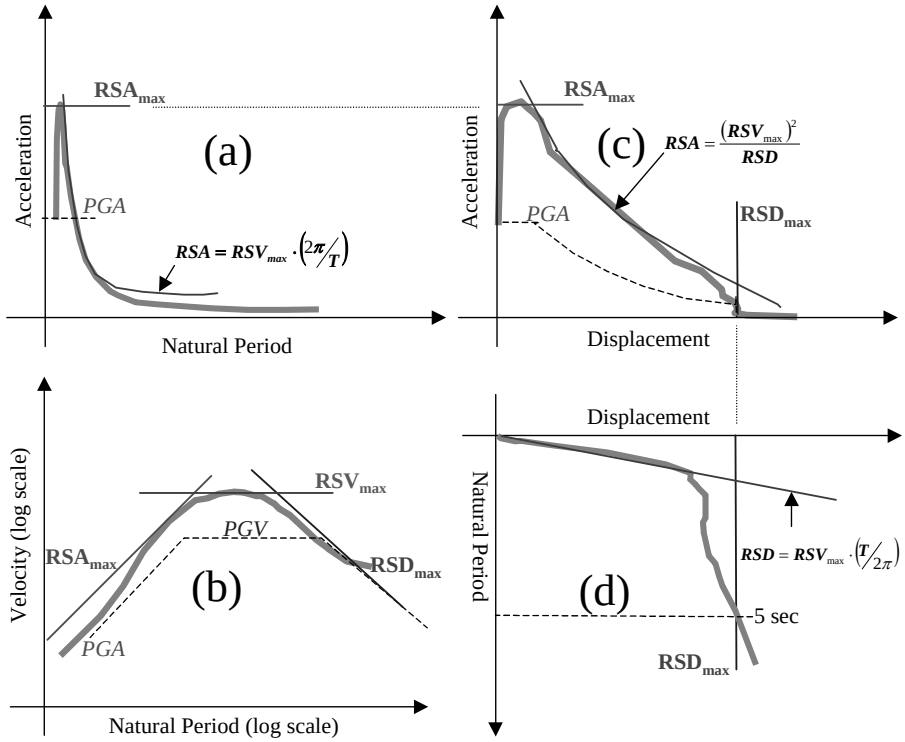

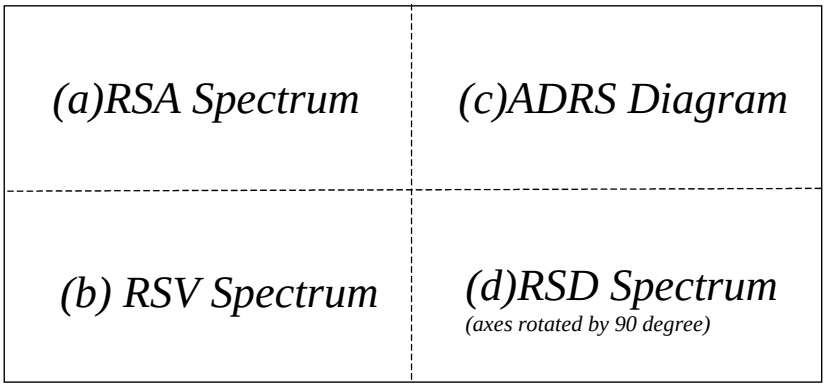

Fig. 5 Response spectrum formats

The displacement model, to be introduced in this paper, is based on the predictions of the $RSD_{\max}$ and $RSV_{\max}$ parameters which jointly control seismic displacement demand. $RSD_{\max}$ is defined at a period of 5 sec (for shaking on the bedrock surface) and at the period of site resonance (T_s) (for shaking on flexible soil). In both the cases, the response spectral displacement can be represented conservatively as a bi-linear function of the system's natural period (*T*) as shown in Figure 5(d).

$$RSD = RSV_{\max} \cdot \frac{T}{2\pi} \tag{1a}$$

$$RSD = RSD_{\max} \tag{1b}$$

whichever is smaller.

In CAM, the displacement parameter of interest ($RSD_{\max}$ and $RSV_{\max}$) is defined by the following expression:

$$RSV_{\max} \text{ or } RSD_{\max} = \alpha.G.\beta.\gamma.S.\psi \tag{2}$$

where

α is the source factor (refer Sub-section 1 in the next section),

G and β are the attenuation factors (refer Sub-section 3 in the next section),

γ is the crustal factor (refer Sub-section 2 in the next section),

S is the site factor (refer the fourth section), and

ψ is the correction factor for equivalent damping other than 5% (refer Sub-section 1 in the fifth section).

The proposed displacement model for intraplate earthquakes is outlined in Figure 6, which has been adopted for comparison with the existing DB procedure shown in Figure 2. A noticeable distinction of the proposed model from existing engineering models is the direct prediction of the displacement demand from geophysical and geotechnical parameters. Thus, the need for converting recorded acceleration to displacement can be avoided. As mentioned earlier, the incorporation of information from local geophysical measurements into CAM makes the model suitable for a diverse range of regional conditions.

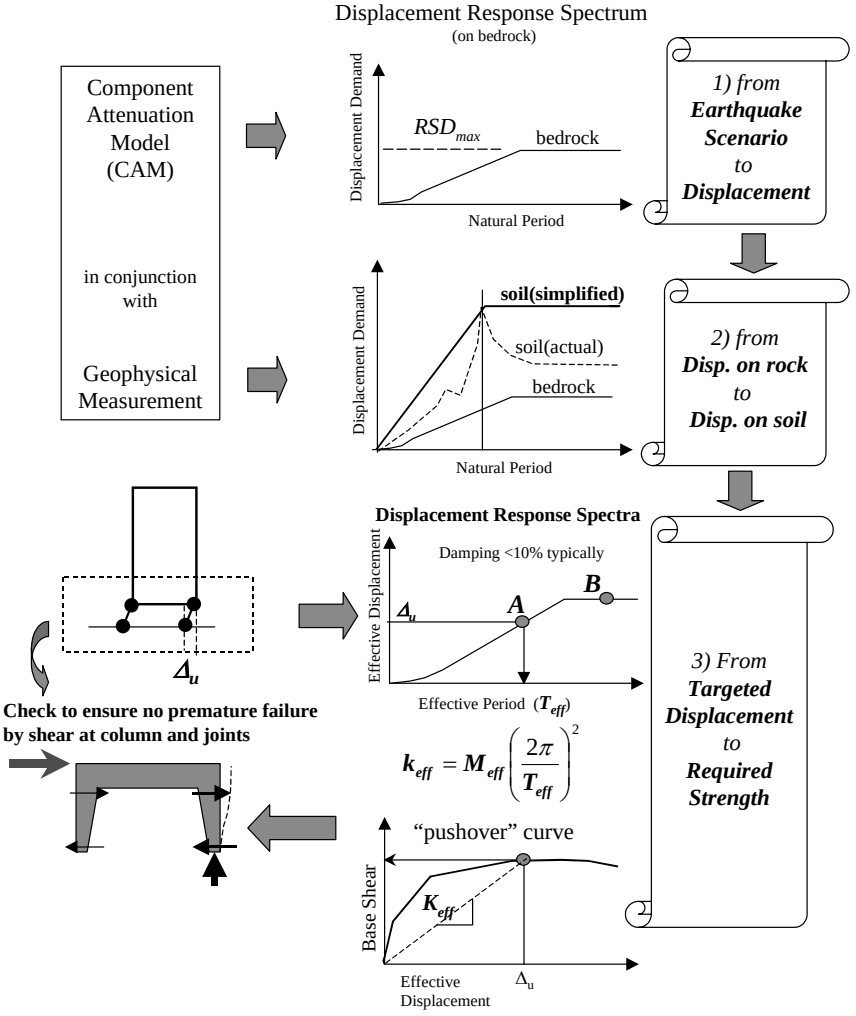

Fig. 6 Framework of proposed intraplate displacement model

DISPLACEMENT MODELLING ON BEDROCK

1. Source Modelling

This section addresses the α factor in Equation (2) which represents the "source" contributions to the displacement demand of a typical intraplate earthquake. The "source" predictions are based on a standard reference distance of 30 km. This source model is based on the generic "Hard Rock" conditions characteristics of the glaciated regions of CENA as defined by Boore and Joyner (1997). In such crustal conditions, the frequency content of seismic waves, generated from the source of the earthquake, is subject only to minor modifications by the surrounding crust which has relatively low energy absorption characteristics. Consequently, the original source properties of the earthquake are largely preserved in motions recorded by seismometers on the ground surface. Thus, seismological models developed for "Hard Rock" sites in CENA can be taken as the source model. However, the CENA source model lacks generality as it is uncertain if the recorded motions are generally representative of intraplate conditions in the global context. Modelling for the $RSD_{\max}$ and $RSV_{\max}$ parameters were undertaken separately.

1.1 Source Modelling for RSD_{max}

A theoretical fault-slip model, which is particularly applicable to small and moderate magnitude earthquakes (M < 6.5), was analysed to develop a generic expression for the peak displacement demand ($RSD_{\max}$) at the source of the earthquake. The merits of adopting a theoretical modelling approach in the development of the source model is the elimination of an intrinsic bias to particular regional conditions. Thus, the developed expression is intended to be applicable to intraplate regions around the world including areas from which little or no strong motion data has been recorded. As shown in the later part of this sub-section, the displacement demand predicted by theory is highly consistent with those predicted by stochastic and empirical models, with the latter developed directly from recorded ground motions (which have been filtered to correct for low-frequency errors in the record).

It has been established by wave-theory that the displacement pulse, *u(t)*, radiated from a small fault rupture is related to the rate of seismic moment release (or seismic moment differentiated with respect to time, $\frac{\partial M}{\partial t}$) by the following expression (Beresnev and Atkinson, 1997):

$$u(t) = \frac{\partial M_o / \partial t}{CR} \tag{3}$$

where

$C = \frac{4\pi\rho V_s^3}{R^{\theta\gamma}}$; $R =$ source-site distance, based on spherical attenuation only,

ρ and V_s are the density and shear wave velocity respectively of the earth crust surrounding the rupture,

$R^{\theta\gamma} \approx 0.78$ is the product of the wave-radiation factor, free-surface factor and energy partition factor.

(Units: M in kg.m^2/sec^2, C in kg/m^3.(m/sec)^3, R in metres => *u(t)* is in metres.)

The rate of seismic moment release can be expressed in terms of the rate of fault-slip, $\frac{\partial \overline{U}}{\partial t}$, as shown by Equation (4):

$$\frac{\partial M_o}{\partial t} = \mu A \frac{\partial \overline{U}}{\partial t} \tag{4}$$

Equation (4) is based on the well known relationship $M_o = \mu A U_\infty$, in which M_o is the total seismic moment.

Solving Equation (4) requires defining the fault slip function $\overline{U}(t)$. The plausible functional form for fault-slip as proposed in Beresnev and Atkinson (1997) is defined by Equation (5):

$$\overline{U}(t) = U_{\infty}\left[1-\left(1+\frac{t}{\tau}\right)e^{-t/\tau}\right] \tag{5}$$

where τ is the time parameter controlling the rate of fault-slip. Differentiating the fault-slip function of Equation (5) with respect to time leads to the slip-rate function:

$$\frac{\partial \overline{U}}{\partial t} = U_{\infty}\frac{1}{\tau}\frac{t}{\tau}e^{-t/\tau} \tag{6}$$

The slip-rate function, $\frac{\partial \overline{U}}{\partial t}$, has a direct physical meaning. According to Equations (3) and (4), $\frac{\partial \overline{U}}{\partial t}$ is proportional to the amplitude of the ground displacement generated by the fault-slip. Substituting Equation (6) into Equation (4) and then into Equation (3) leads to Equation (7) which defines the displacement time-history, *u(t)*, of the generated pulse:

$$u(t) = \frac{M_o}{CR}\frac{1}{\tau}\frac{t}{\tau}e^{-t/\tau} \tag{7}$$

To obtain the peak ground displacement $U_{\max}$, Equation (7) will have to be differentiated with respect to time to locate the peak in the time domain:

$$\frac{\partial u(t)}{\partial t} = \frac{M_o}{CR}\frac{1}{\tau}\left(\frac{1}{\tau}-\frac{t}{\tau^2}\right)e^{-t/\tau} \tag{8}$$

From Equation (8), the generated ground displacement reaches its peak value $U_{\max}$ when $t = \tau$. Thus, $U_{\max}$ can be estimated by substituting $t = \tau$ into Equation (7), which leads to Equation (9):

$$U_{\max} = \frac{M_o}{CRe\tau} \tag{9}$$

where e is the exponential function.

It can be shown that (Lam and Chandler, 2004):

$$\tau \approx 0.37\frac{\left(\frac{M_o}{\Delta\sigma}\right)^{1/3}}{V_s} \tag{10}$$

where $\Delta\sigma$ is the stress-drop and V_s is the shear wave velocity.

Substituting Equation (10) into Equation (9) leads to an expression (not shown) which defines the value of $U_{\max}$ (or *PGD*) in terms of the seismic moment (M_o), stress-drop $(\Delta\sigma)$, shear wave velocity (V_s), crustal density (ρ) and source-site distance (R). This expression is reduced to Equation (11a) if the parameter values recommended for generic "Hard Rock" by Atkinson and Boore (1995) have been substituted into the expression:

$$PGD = 8.7\times10^{-15}\left(M_o\right)^{2/3} \tag{11a}$$

where *PGD* is in metres and M_o in N-m.

Given that, by definition: $M_o(\text{dyne-cm}) = 10^{1.5M+16.05}$ or $M_o(\text{N-m}) = 10^{1.5M+16.05-7}$ (Kanamori, 1993), Equation (11a) can be rewritten as:

$$\log_{10}(PGD) \approx -14 + \tfrac{2}{3}(1.5M + 16.05 - 7) \tag{11b}$$

$$PGD\ (\text{in m}) \approx 10^{M-8} \tag{11c}$$

or

$$PGD\ (\text{in mm}) \approx 10^{M-5} \tag{11d}$$

where M is the moment magnitude.

A more detailed description of the theoretical derivation for Equations (10)-(11) can be found in Lam and Chandler (2004).

The ground displacement time-history associated with the adopted fault-slip function is represented graphically in Figure 7(a). The highest point on each of these time-histories is the peak ground displacement (*PGD)*. Response spectrum analysis has then been undertaken for each of the idealised displacement time-histories to produce the theoretical displacement response spectra, as shown in Figure 7(b). The highest point on the displacement response spectrum up to a natural period of 5 sec is defined herein as the peak displacement demand $(RSD_{\max})$. Predictions for the *PGD* and $RSD_{\max}$ are generally very similar. Thus, predictions for $RSD_{\max}$ can be made using Equation (11).

It is important to note the limitations of this theoretical fault-slip model which is based on the assumption of a smooth time-displacement function that is free of any major irregularities such as the breaking up of one continuous fault-slip into numerous smaller slips. For example, two pulses generated by the earthquake source at a period interval of 1 sec could induce significant response amplification in systems possessing a similar natural period of vibration. The engineering significance of this "periodicity" effects of the source increases with the duration of rupture since pulses arriving at longer time intervals (i.e. longer periods) are more damaging. Consequently, the theoretical model in which the periodicity effects have been ignored will have limitations with the modelling of large magnitude earthquakes which are characterized by a long rupture duration. Predictions based on the analysis of a theoretical fault-slip function on its own is, therefore, unreliable and must be supported by predictions developed from empirical strong motion models and from stochastic simulations of seismological models (also known as "semi-empirical" models).

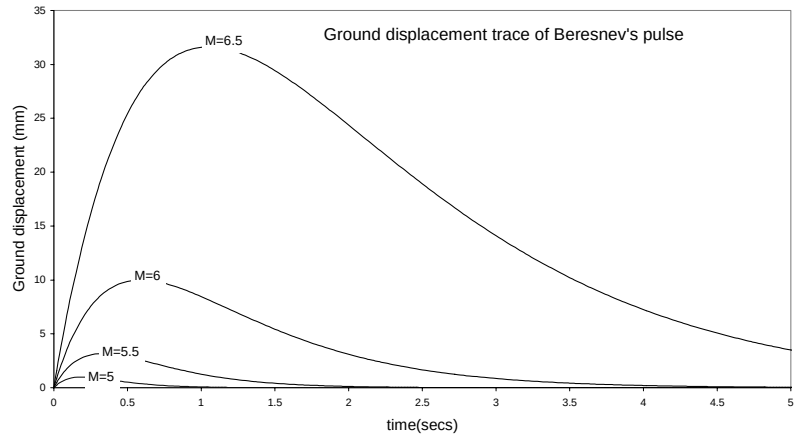

(a)

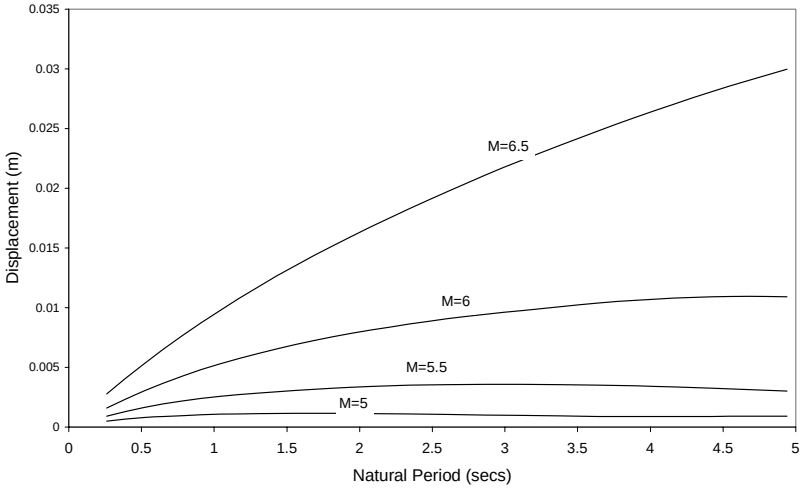

(b)

Fig. 7 Theoretical displacement demand predictions after Lam and Chandler (2004)

Both the *PGD* and $RSD_{\max}$ parameters, developed from the theoretical fault-slip models, are plotted in Figure 8(a) as a function of earthquake magnitude along with empirical predictions by Abrahamson and Silva (1997). The Abrahamson model is amongst the very few empirical models that have the exceptional quality of predicting response spectrum up to a natural period limit of 5 sec (at which $RSD_{\max}$ is defined) due to the extra filtering that have been undertaken to correct errors at the high period end of the spectrum. The other empirical model, that has been subject to similar corrections and provides similar displacement predictions (at T = 5 sec), is the response spectrum model developed independently by Bommer and Elnashai (1999). Note, predictions by both models have been corrected by a crustal factor of 1.5 (refer Sub-section 2.3 for justification).

Also included in the comparison is the CAM expression introduced by the authors in their earlier publication (Lam et al., 2000a). This earlier recommendation by the authors was based on stochastic simulations of the empirical source model developed by Atkinson (1993) from seismometer data collected in CENA (refer Lam et al. (2000d) for details of the simulation process). As shown in Figure 8(a), Equation (11) is very close to this earlier presented CAM expression and is much simpler.

Further details of an extensive comparative study in support of the predictions by the theoretical fault-slip model can be found in Lam and Chandler (2004). For moment magnitude up to 6-6.5, the peak displacement demand ($RSD_{\max}$) of the source, as predicted by Equation (11), was found to be within 5 mm of all the other predictions included in the comparison as shown in Figure 8(a).

1.2 Source Modelling for RSV_{max}

It is evident from the comparative study reported above that seismological models, based on CENA conditions, may be used to generalise the source behaviour of intraplate earthquakes. The generality of the two CENA models (Atkinson, 1993; Toro et al., 1997 respectively) is further confirmed by the comparison of their predicted peak velocity demand ($RSV_{\max}$) with that of the model by Dahle et al. (1990) for the Scandinavian peninsular, the Intensity model by Gaull et al. (1990) for Western Australia, and the CAM model by Lam et al. (2003a) for the whole of Australia. Conditions akin to ancient (pre-Cambrian) geological formations like CENA were considered in these studies. In view of the very good consistencies between the predictions as shown in Figure 8(b), the authors re-affirmed their earlier CAM expressions for $RSV_{\max}$ in Lam et al. (2000a, 2000b) as the generic expression for the source contributions to intraplate earthquakes. This earlier CAM expression is re-stated in Equation (12).

$$RSV_{\max}(\text{mm/sec}) = 70\left(0.35 + 0.65\left(M - 5\right)^{1.8}\right) \tag{12}$$

In summary, the source contributions to the velocity-displacement response spectral demand of an intraplate earthquake is given by Equations (11) and (12) along with Equations (1) and (2).

2. Crustal Modelling

This section addresses the γ factor in Equation (2), which represents the crustal contributions to the seismic displacement demand. The γ factor can be resolved further into the mid-crust factor γ_{mc} and the upper crust factor γ_{uc} as described in the following sub-sections.

2.1 Mid-Crust Factor

The amplitude of seismic waves generated at the source of an earthquake is proportional to the shear wave velocity (V_s) of the surrounding crust raised to the power of 3 according to wave theory. Implicit in the derivation of Equations (11) and (12) is the assumption that V_s is equal to 3.8 km/sec which is representative of conditions at a depth (d) exceeding 12 km. At a shallower depth d = 4-8 km, V_s is estimated to average at around 3.5 km/sec based on the generic shear wave velocity profile of Boore and Joyner (1997). For most moderate and large magnitude shallow earthquakes ($M \geq 6$), the centroid of the ruptured surface is constrained to a depth of at least around 5 km (for a rupture area of 100 km^2 even if the rupture is assumed to have reached the earth surface). The "mid-crust" factor introduced herein, which allows this depth effect of the source, is accordingly 1.3 (being 3.8/3.5 raised to a power of 3).

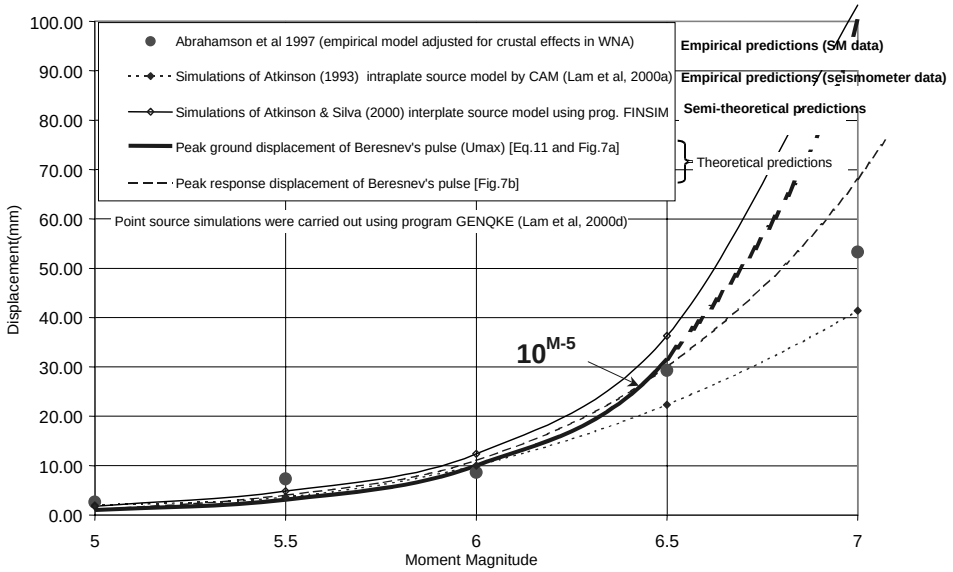

(a)

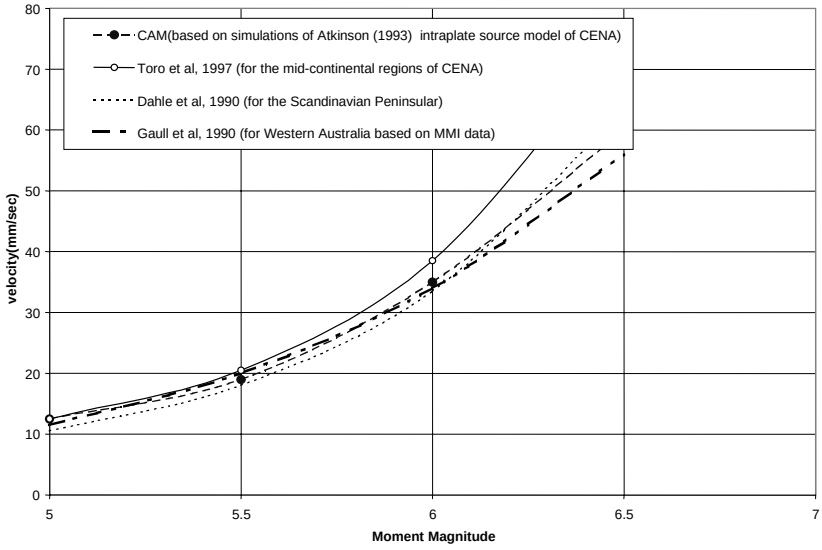

(b)

Fig. 8 Comparisons of theoretical, empirical and stochastic predictions after Lam and Chandler (2004): (a) displacement, (b) velocity (mm/sec)

2.2 Upper-Crust Factor

Upward propagating seismic waves can be modified rapidly by the upper (say 4 km) layers of the earth's crust partly due to the shear wave velocity gradient. The seismic waves could also be affected significantly by attenuation mechanisms which are represented collectively by the well known *kappa* parameter (Anderson and Hough, 1984; Atkinson and Silva, 1997; Abercrombie, 1997; Boore and Joyner, 1997). These path effects as described can be difficult to track if measurements are only taken from the earth's surface. A viable, but very expensive, method in studying crustal properties is by drilling and instrumenting boreholes several kilometres deep into the ground (e.g., Abercrombie, 1997).

Generic crustal shear wave velocity profiles have been developed by Boore and Joyner (1997) for both Western North America (WNA) and CENA using a large database of downhole travel time survey

records along with P and S-waves velocity data obtained from seismological refraction experiments and monitoring programs (refer Figure 9(a)). The proposed "quarter wave length approximation" rule was applied on the modelled shear wave velocity profiles to determine the filter function for upper crustal amplifications.

As the shear wave velocity gradient induces amplifications in the seismic waves, energy absorption in the young "soft" upper crust causes significant attenuation. The attenuation properties of the upper crust is represented by the *kappa* parameter in seismological research literature (e.g., Atkinson and Silva, 1997). The value of *kappa* is estimated to be in the range 0.05 sec for WNA (Atkinson and Silva, 1997) but lower values are expected in mid-continental (intraplate) regions. Stochastic simulations have been used to represent the combined effects of the upper crustal amplification and attenuation in the form of the velocity response spectrum. The decrease in sensitivity of amplification to increasing period of the wave components is observed (refer Figure 9(b) for analysis results based on the earthquake scenario of *M*6 at an hypocentral distance of 30 km on rock sites).

The influence of *kappa* on the response spectrum is also shown to diminish rapidly with increasing natural period. Consequently, displacement demand is more robust to model than the acceleration demand. The peak response spectral amplification is shown to occur at the period range of 0.2-0.6 sec. Wave components in this period range are controlled by properties of the earth crust at a depth range of between 100-400 m according to the quarter-wave length approximation rule. Drilling holes to this depth for "down-hole" or "cross-hole" surveys are very expensive and is rarely undertaken in intraplate regions. Conventional seismic reflection and refraction techniques typically provide information on the compressive (P) wave velocity only and not the shear wave (S) velocity. Measurement of *kappa* can be undertaken by monitoring the decay of Coda Waves but the need to focus on the upper 4 km or so of the earth crust means that measurements are required from an epicentral distance of less than 5 km. In summary, modelling upper crustal factors from first principles using conventional monitoring methods is faced with serious practical problems.

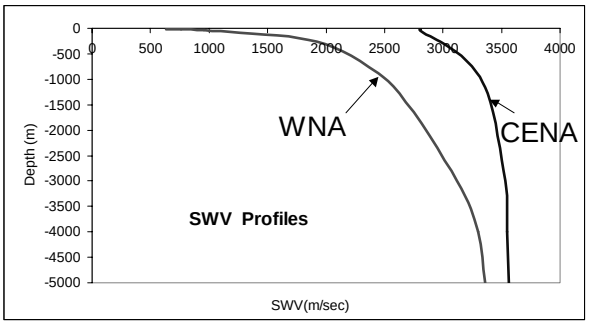

(a)

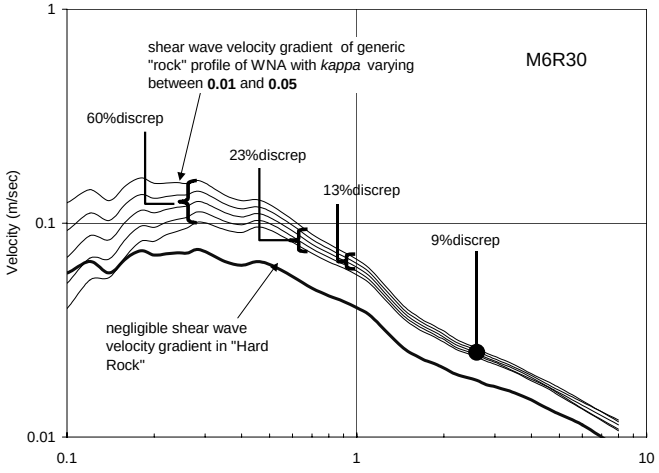

(b)

Fig. 9 Upper crust model

An inexpensive innovative procedure under development to measure regional crustal properties uses the microtremor wave field (seismic energy generated by road traffic, machinery, and meteorological sources such as wave action at coast-lines). Observations are made using typically seven seismometers in small circular arrays of diameter 10 to 200 m, and processed using the spatially averaged coherency (SPAC) method. The technique requires no drilling and yields estimates of thickness and shear-velocity of soil and rock in order that crustal amplification can be modelled (Asten and Dhu, 2002; Asten et al., 2002; Asten, 2003). Crustal attenuation (as represented by the *kappa* parameter) could then be estimated by calibration with results obtained from shear wave analysis of the measured shear wave velocity profile. The calibrated correlation between *kappa* and the crustal shear wave velocity will become part of CAM. This new approach of measurement and modelling, which integrates SPAC with CAM, is currently under development.

2.3 Combined Crustal Factor

Ideally, crustal factors should be based wholly on local geophysical measurements and the wave modification mechanisms described above (in Sub-section 2.1-2.2). However, a practical and comprehensive measurement-modelling methodology, suited for worldwide applications, has yet to be fully developed. In the interim, useful benchmarks for estimating the crustal factors can be obtained by collating and comparing attenuation relationships developed for different regions. The "combined crustal factors" inferred from these comparative analyses have incorporated the effects of all amplification and attenuation mechanisms affecting the earthquake. A multitude of studies included in this inference analysis is described below under separate sub-headings (based on earthquake scenarios of *M*5-*M*5.5 at 30 km hypocentral distance):

(a) Studies by the Authors: The value of γ_{uc} associated with the peak velocity demand $(RSV_{\max})$ was estimated at around 1.2 for *kappa* = 0.05. The combined mid-crustal factor (γ_{mc}) and upper-crustal factor (γ_{uc}) is accordingly 1.6 (being the product of 1.3 and 1.2). More recent analyses by the authors (Lam et al., 2003a) reported the increase of γ_{uc} to 1.5 when assuming a lower *kappa* value of 0.03. The combined crustal factor is accordingly equal to 2. Importantly, the value of γ_{uc} at the 5 sec period which controls the peak displacement demand $(RSD_{\max})$ is very insensitive to *kappa* and remains constant at around 1.25. The corresponding combined crustal factor is 1.6.

(b) Studies by Gaull et al. (1990): Information from Iso-seismal maps collected from a number of Australian earthquakes including the *M*6.9 Meckering earthquake of 1969 and the *M*6.2 Cadoux earthquake of 1979 have been used to study earthquake attenuation behaviour (Gaull et al., 1990). In view of variations in crustal properties across the continent, separate attenuation relationships were developed for Western Australia (which pertains to "Hard Rock" conditions) and for South-Eastern Australia (which pertains to "Rock" conditions). The Intensity values modelled for the two regions could be translated into peak ground velocities (*PGV*s) using the Newmark and Rosenblueth (1971) expression. Although this expression was originally developed from field observations in Western US, it has been found to be equally applicable to South China (Chandler and Lam, 2002) and different regions within Australia (Lam et al., 2003a). Ratios of the *PGV*s predicted for the adjacent regions (of different geological formations) can be taken to be directly indicative of the combined crustal effects given that their source characteristics should be similar. The inferred crustal factor is in the range 1.56-1.58. The effects of surface soil amplifications, which are implicit in the Intensity data, are assumed to have been eliminated in the ratios.

(c) Studies by Toro et al. (1997): The continental region of CENA and the adjacent "Mexican Gulf" regions modelled by Toro are expected to have similar source characteristics, being adjoining regions in CENA. Thus, again, the ratios of their *PGV*s predicted for rock sites in the two regions could be taken as indicative of the combined crustal effects in the "younger" crustal region surrounding the Mexican Gulf. The inferred crustal factor is in the range of 1.54-1.62.

(d) Studies by Atkinson and Boore (1998): Combined crustal factors for WNA have also been analysed by Atkinson based on stochastic simulations of the crustal model developed by Boore and Joyner (1997). Note, the seismological parameters used in this study and that by the authors are the same, however, the simulations and response spectral computations were undertaken independently using different software programs. The inferred crustal factor is in the range of 1.35-1.82.

(e) Comparison of Model by Sadigh et al. (1997) and Toro et al. (1997): These two models are well known attenuation models that were developed independently for WNA and CENA respectively. Combined crustal factors in the range of 1.03-1.12 were inferred by taking the ratio of the highest velocity demand predicted by the two models for rock sites in identical earthquake scenarios.

The following table provides a summary of the combined crustal factor obtained from the enlisted studies. The predictions were based on earthquake scenarios of *M*5.5-*M*6.5 at 30 km distance on rock sites. The period range of interest is 0.2-0.6 sec which controls the peak velocity demand $RSV_{\max}$.

Table 1: Combined Crustal Factor (γ) for $RSV_{\max}$ Inferred from Different Studies

Study	Basis of the Crustal Factor γ	γ
(a) Lam et al. (2000a) Lam and Wilson (2003)	"Hard-Rock" versus "Rock" *kappa* averaged at 0.05 *Kappa* = 0.03	 1.6 2.0
(b) Gaull et al. (1990)	Western Australia versus South-Eastern Australia	1.56-1.58
(c) Toro et al. (1997)	Mid-continental CENA versus Mexican Gulf region	1.54-1.62
(d) Atkinson and Silva (1997)	"Hard-Rock" versus "Rock"	1.35-1.82
(e) Sadigh et al. (1997) and Toro et al. (1997)	WNA versus CENA	1.03-1.12

The crustal factors listed in Table 1 based on the different studies are generally consistent except for "(e)" which shows much lower values. This apparent anomaly can be explained by the partial trade-offs of the crustal effects with the effects of a lower stress-drop associated with interplate earthquakes in WNA. Consequently, it is not always conservative to adopt attenuation models developed in interplate regions of high seismicity for applications in intraplate regions of low-moderate seismicity.

In the absence of sufficient reliable local information for the determination of the individual crustal factors (refer Sub-sections 2.1 and 2.2), an assumed combined crustal factor of 1.5-1.6 seems reasonable for the modelling of both $RSD_{\max}$ and $RSV_{\max}$ in young geological conditions and is in alignment with various attenuation relationships considered in this review. A higher value of γ (= 2.0) obtained from stochastic simulations based on *kappa* = 0.03 (refer case "(a)" in Table 1) is plausible but the γ value is significantly higher than that inferred from existing attenuation relationships. The discrepancies can be explained by the difference in energy absorption properties of the crust and the different level of ground motion intensities implicitly assumed in the various attenuation models. In theory, an even lower *kappa* value (< 0.01) is possible but the shear wave velocity gradient in such conditions is unlikely to result in an even higher crustal factor.

In summary,

γ = 1.0 deep events (d > 10 km) in *Hard Rock* conditions typical of the CENA region (and similar regions of pre-cambrian formation; e.g. parts of Western Australia) (13a)

γ = 1.3 shallow events in *Hard Rock* conditions (mid-crust amplification only) (13b)

γ ~ 1.5–1.6 shallow events in young geological formations typical of continental margins (e.g. WNA) with *kappa* ~ 0.05 assumed (13c)

γ ~ 2.0 similar conditions as above but with a low *kappa* value of 0.03 (13d)

(Refer Figure 9(a) for the shear wave velocity profile assumed for the conditions of "CENA" and "WNA")

3. Attenuation of Distant Earthquakes

This section addresses the G factor and the β factor in Equation (2) which represents the effects of geometrical and anelastic whole path attenuation respectively. For near-field earthquakes (R < 50 km), the G and β factors (both normalised to unity at 30 km distance) is given by Equation (14) (Lam et al., 2000a, 2000b).

$$G(R) = 30/R \qquad (\text{for } R \le 50\,\text{km}) \tag{14a}$$

$$\beta(R) = (30/R)^{C_1 R} \qquad (\text{for } R \le 50\,\text{km}) \tag{14b}$$

where C_1 = 0.003 and 0.005 for $RSD_{\max}$ and $RSV_{\max}$ respectively.

At this distance range, regional differences are not shown to significantly effect the attenuation of the seismic waves. With short wave transmission path, energy dissipation is generally very limited and hence regional parameters have not been incorporated into the expression. As the wave transmission path exceeds 100 km, regional parameters such as the depth to the "Moho" discontinuity (*D*) and Quality Factor (*Q*) become significant.

Low amplitude seismometer records may contain potentially useful information of the wave travel path regardless of the engineering significance of the earthquake itself. For example, the attenuation of low amplitude seismic waves with distance (spectral-ratio method) and time (Coda Q method) is commonly measured using seismometers (Wilkie and Gibson, 1995). The Quality Factor (*Q*) determined from these studies defines the regional wave transmission quality of the earth's crust. Whilst the measurement seems relatively straightforward, results are typically interpreted only in terms of a filter function in the Fourier spectral format. Importantly, there has been no widely recognised, and direct, link between *Q* and the potential earthquake hazard in direct engineering terms such as the response spectrum parameters $RSA_{\max}$, $RSV_{\max}$ and $RSD_{\max}$ (other than by repetitive stochastic simulations using specialised software).

The G factor in Equation (14a) has been modified in accordance with the tri-linear attenuation relationship of Atkinson and Mereu (1992). Equation (14b) has also been further developed into a far more elaborate form to provide the link between the β factor and the Q factor (Lam et al., 2002). The developed attenuation relationships are presented herein graphically (Figures 10(a) and 10(b)). The latter figure is primarily intended for modelling the anelastic attenuation of long period wave components that control the peak displacement demand $RSD_{\max}$ as defined in Equation (2). Estimating the anelastic attenuation of $RSV_{\max}$ involves the use of a less conservative function (Lam et al., 2002).

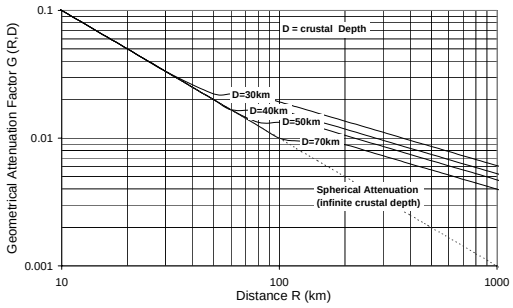

(a)

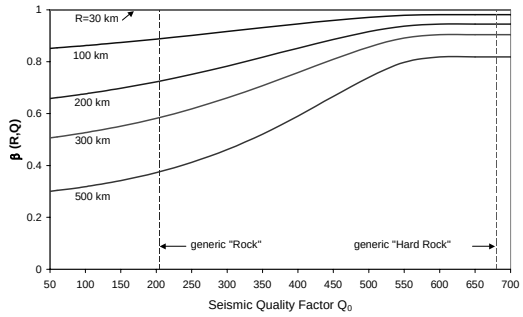

(b)

Fig. 10 Geometrical and anelastic attenuation of displacement demand (after Chandler and Lam (2004))

The proposed attenuation relationships have been verified by comparison with field observations from recent major earthquake events around the globe including the Chi-Chi (Taiwan) earthquake in 1999, the Nisqually (Seattle) earthquake in 2001, the Gujarat earthquake (India) in 2001, and distant earthquakes affecting Singapore in 1996 and 2000. Further, Chandler and Lam (2004) presents a detailed description of the field-model comparisons, which provide support for the proposed attenuation model for distant earthquakes. Additional support for the model is provided from both instrumented and intensity data collected from the Sumatran-Singaporean region (Balendra et al., 2002).

4. Displacement Spectrum and Corner Period

The displacement demand for intraplate earthquakes of any given magnitude-distance (*M-R*) combination on rock sites can be predicted using Equations (1) and (2) in conjunction with Equations (11)-(14) and Figures 10(a)-10(b). The $RSV_{\max}$ and $RSD_{\max}$ parameters calculated from the displacement model can be used to construct a simplified bi-linear response spectrum in accordance with Equation (1) in order that the displacement demand can be estimated for any given natural period of the structure. Although the response spectrum construction may appear overly-conservative in the *RSA* and *RSV* formats (Figures 11(a)-11(b)), it matches the actual response spectrum very closely when presented in the *ADRS* or *RSD* formats (Figures 11(c)-11(d)). Although the constructed ADRS diagram may also appear very conservative at small displacement, the conservatism has little significance in practice given that most capacity curves are characterised by stiffness deterioration (hence reduced acceleration demand) with increasing displacement as shown in Figure 11(c).

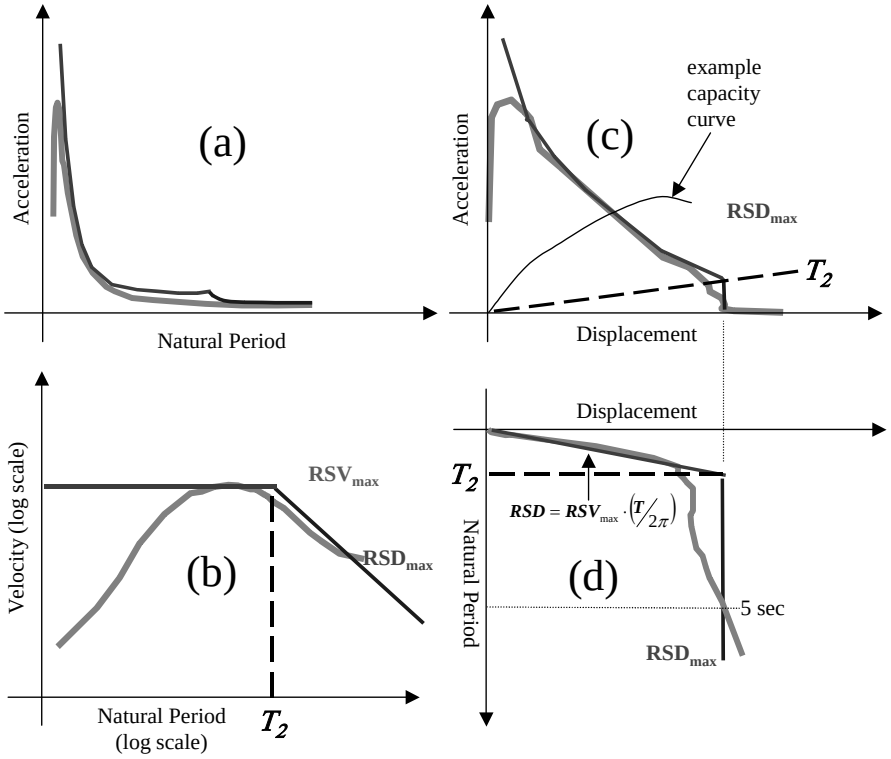

Fig. 11 Bi-linear displacement model (presented in different formats)

Central to the construction of the simplified response spectrum is the corner period (labelled as T_2 in Figure 11). The value of T_2 can be calculated using Equation (1) when both $RSV_{\max}$ and $RSD_{\max}$ have been determined by the displacement model.

However, in situations where specific *M-R* combinations have not been identified (and consequently the dual parameters cannot be calculated), the value of T_2 will have to be assumed. T_2 allows the simplified response spectrum to be constructed for any given design *PGV*. For example, a consensus on the design *PGV* for different parts of Australia has been reached for return periods varying between 500-2500 years. *PGV* contour maps are already available for the whole of Australia but a realistic response

spectrum model will need to be developed for incorporation into any new earthquake loading standard. The peak velocity demand (RSV_{max}) can be estimated using Equation (15).

$$RSV_{max} = c.PGV \tag{15}$$

where c equals "1.8" according to Somerville et al. (1998), and "2" according to Lam et al. (2000a).

Given RSV_{max}, the value of RSD_{max} can be calculated using Equation (1) assuming T_2 = 1.5 sec. This simplified response spectrum construction, as proposed by Wilson and Lam (2003), is the basis of the draft response spectrum provision for rock sites in the new standard (refer Figure 12).

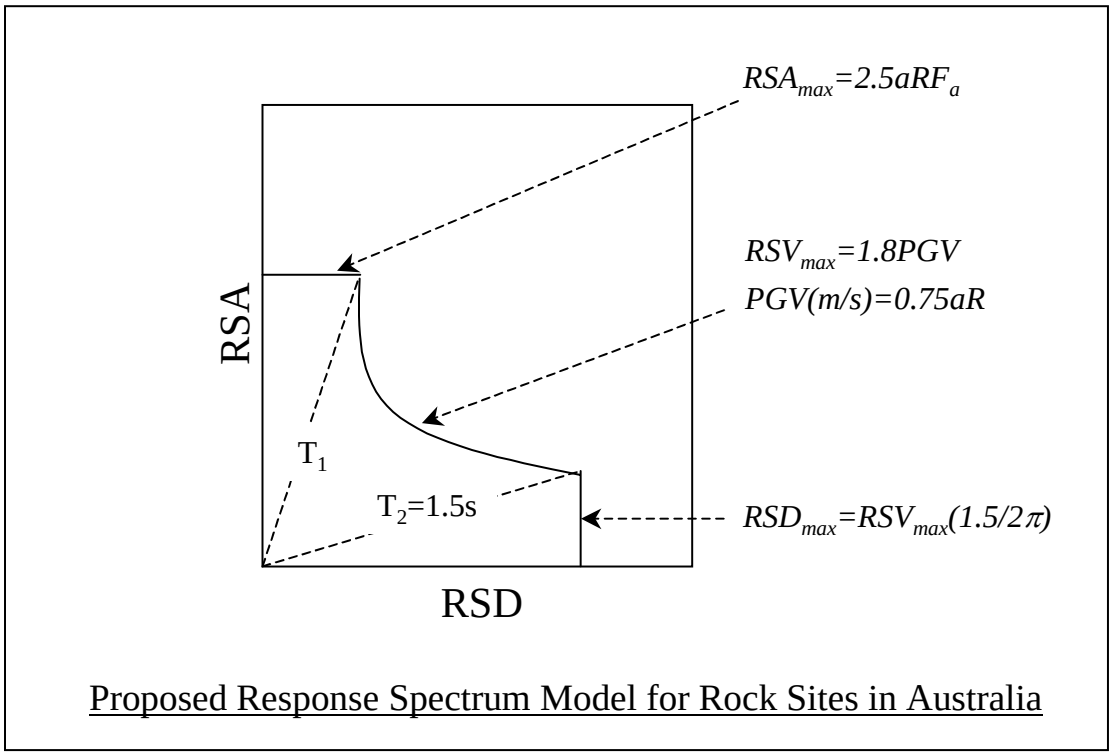

Fig. 12 Scaling of the response spectrum by the peak ground velocity (after Wilson and Lam (2003))

The corner period has been used in other codes of practices for earthquake loading in their response spectrum provisions. In Eurocode 8-2001, T_2 = 2 sec was used to "cap" the predicted displacement demand.

It can be shown that the actual value of T_2 is very sensitive to crustal conditions and moment magnitude (*M*), with T_2 increasing with increasing value of *M*. The assumption of T_2 = 1.5-2 sec is generally consistent with the proposed displacement model for *M6.5-M7* earthquakes. Note, the response spectrum model for Australia, as shown in Figure 12, is based on a maximum credible earthquake (MCE) of *M7*. A less conservative T_2 value as defined by Equation (16) which was first introduced in Lam et al. (2000b, 2000c) may be used for earthquakes of smaller moment magnitude.

$$T_2 = 0.5 + 0.5\left(M - 5\right) \tag{16}$$

The corner period may also be used in a "reverse" procedure for the response spectrum modelling of distant earthquakes. In the reverse procedure, RSD_{max} is first determined using Equations (11) and (13) and Figures 10(a)-10(b). T_2 is then determined using Equation (16). The values of both RSD_{max} and T_2 are then substituted into Equation (1) to predict the value of RSV_{max} and to complete the construction of the response spectrum. Understating the corner period in this reverse procedure will result in the construction of a more conservative response spectrum. (Note, anelastic attenuation over long distance

would increase the value of T_2, since higher period wave components are subject to less attenuation than lower period wave components. Consequently, the use of Equation (16) in the reverse procedure should give conservative response spectrum estimates for distant earthquakes.)

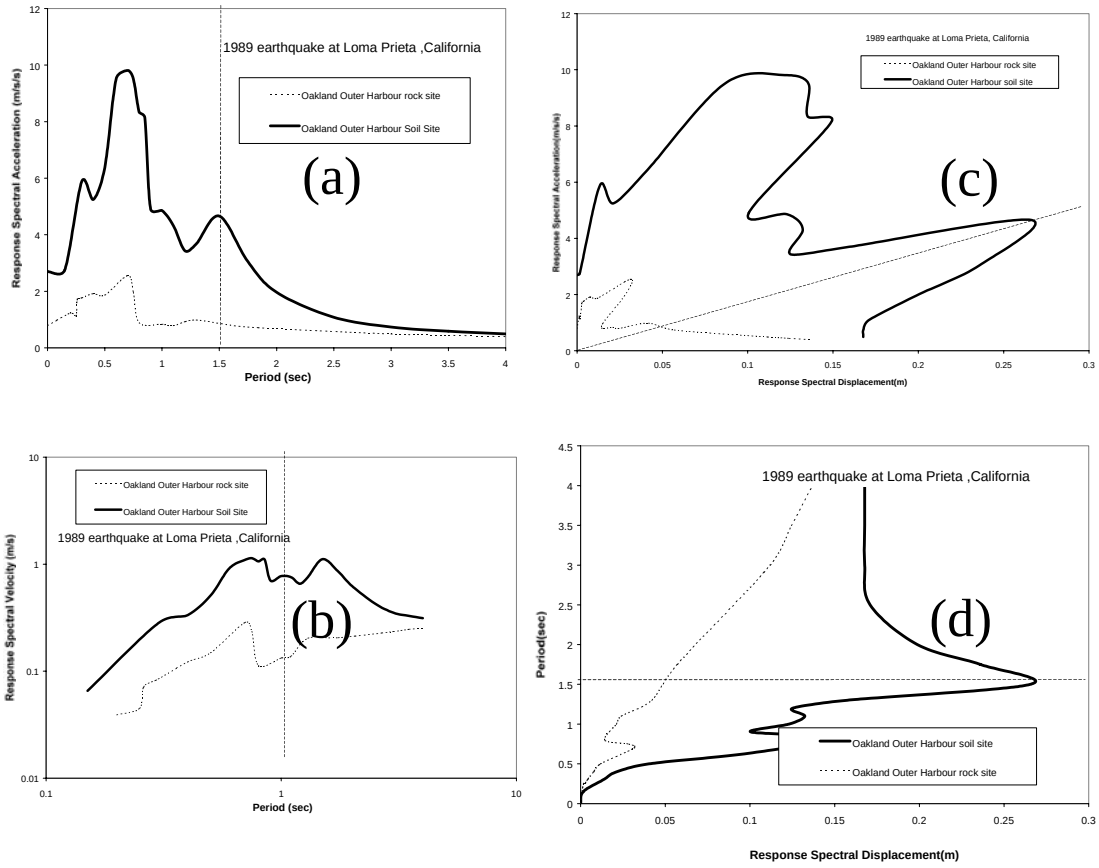

Fig. 13 Response spectra showing the effects of resonance

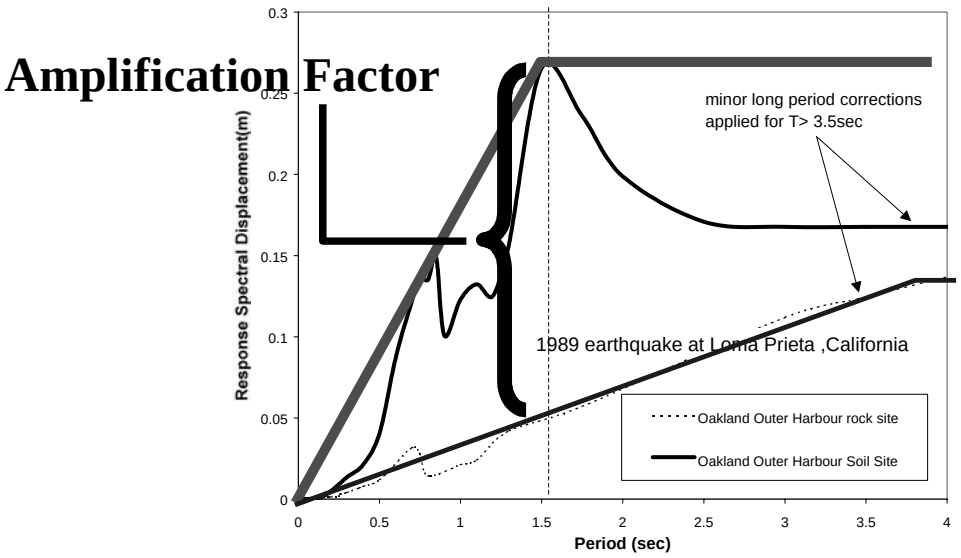

Fig. 14 Definition of the soil amplification factor

DISPLACEMENT MODELLING ON SOIL

Displacement amplification of structures on flexible soil (i.e. site natural period > 0.6 sec) is an important issue in intraplate regions where structures typically possess limited ductility and energy dissipation capacity to suppress the effects of soil-structure resonance. In theory, the natural period of the structure and that of the soil could be compared to ensure that large site amplification pertaining to "resonance" conditions would not occur. The natural period of the soil could be measured by micro-tremor monitoring or by analysis of borehole records (Lam and Wilson, 1999). However, in practice, the natural period of the structure as indicated by the computer model might not be realistic due to over-simplifications in the modeling (which often neglects the complex interaction of the structure with non-structural components including partitions and facades). Furthermore, reinforced concrete structures that have cracked will exhibit non-linear behaviour resulting in a significant period-shift even when responding within notional yield limits (refer Sub-section 2 in the fifth section). Structures might experience resonance if the period-shift is enough to draw the initial natural period of the structure close to the site natural period.

The RSD spectrum is considered to best represent amplification of the displacement demand by resonance (Figure 13(d)) in comparison with other response spectrum formats (Figures 13(a)-13(c)). The example spectra are based on the ground motion recorded on a soft soil site at Oakland Harbour during the 1989 Loma Prieta earthquake as reported by Dickenson et al. (1991). The displacement spectrum can be simplified into a bi-linear model as shown in Figure 14. Central to the construction of the bi-linear model is at the corner of the spectrum where the pre-determined fundamental site period (T_s) and the associated highest displacement demand $(RSD_{\max})$ are shown. The soil amplification factor "*S*" in Equation (2) is based on this displacement demand. This concept of defining soil amplification was first proposed in Lam et al. (2001).

Soil amplification are widely known to be controlled by both the soil shear wave velocity profile and damping. Codes of practices typically classify sites according to the average shear wave velocity in the upper soil layers (e.g., IBC, 2000; AS1170.4, 1993) or the site natural period (e.g., NZ4203, 1992). The site natural period has been used as the key parameter in micro-zonation studies to characterize site seismic hazard. According to the displacement model shown in Figure 14, the peak displacement demand $(RSD_{\max})$ would increase linearly with increasing site period (T_s) even if the S factor is kept constant. Consequently, the damage potential of an earthquake increases with T_s (due to the fact that higher period seismic wave components have been amplified). Interestingly, there are also noticeable influences on the *S* factor by the shape of the shear wave velocity profile of the soil as revealed from a recent study by Venkatesan (2004) based on analyses using program SHAKE (Idriss and Sun, 1991). It is shown in Figures 15(a)-15(c) that the average soil amplification factor for "irregular", "linear" and "polynomial" shear wave velocity profile is respectively 1.3, 1.4 and 1.5 times higher than that for the reference "uniform (weighted average)" shear wave velocity profile. These factors are based on the site natural period being kept constant. This "profile shape" effect is represented herein by the factor S_ψ.

Trends related to the effects of hysteretic damping and radiation damping have also been studied by Venkatesan et al. (2003). The decrease in the value of the soil amplification factor with increasing *PGV* of the bedrock, as shown in Figure 16, was attributed to hysteretic damping in the soil. An approximately 1/3-1/2 unit change in the soil amplification factor for every 50 mm/sec change in the bedrock *PGV* is indicated. The factor S_ξ is introduced herein to account for this damping effect.

The effects of radiation damping at the soil/rock interface (as distinct from hysteretic damping within the soil) is accounted for by another factor S_λ. The higher the shear wave velocity of the bedrock, the lower the level of radiation damping and consequently the higher the seismic displacement demand. As shown in Figure 17, some 25% increase in the displacement demand on the soil surface is estimated when the bedrock shear wave velocity has been increased from 1000-2000 m/sec. A simple, and conservative, expression for the S_λ factor has been developed initially by Chandler (2003) (and modified by Venkatesan (2004)).

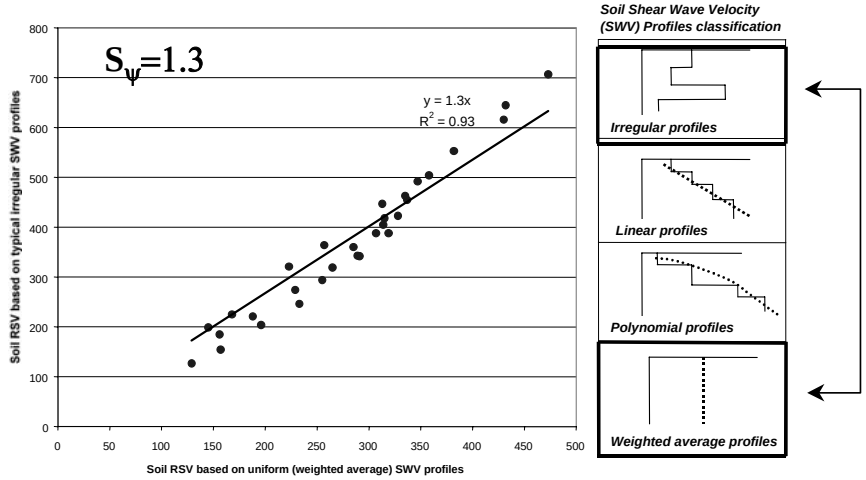

(a) Typical Irregular versus Uniform SWV profiles

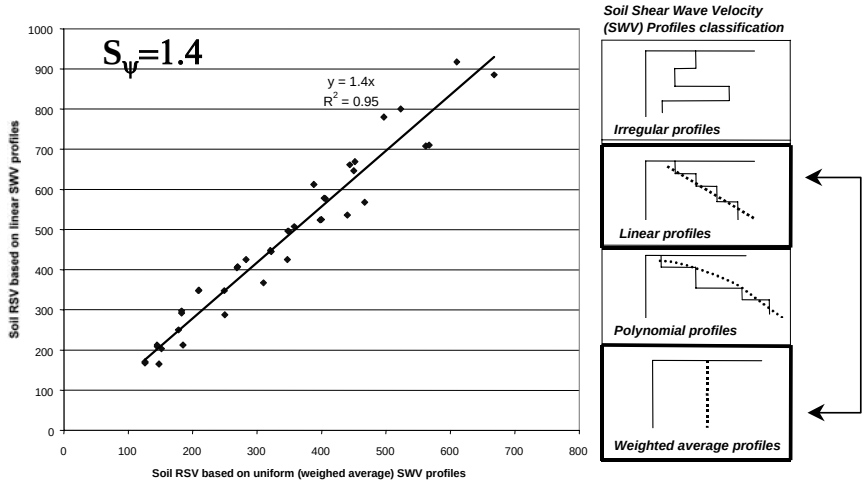

(b) Linear versus Uniform SWV profiles

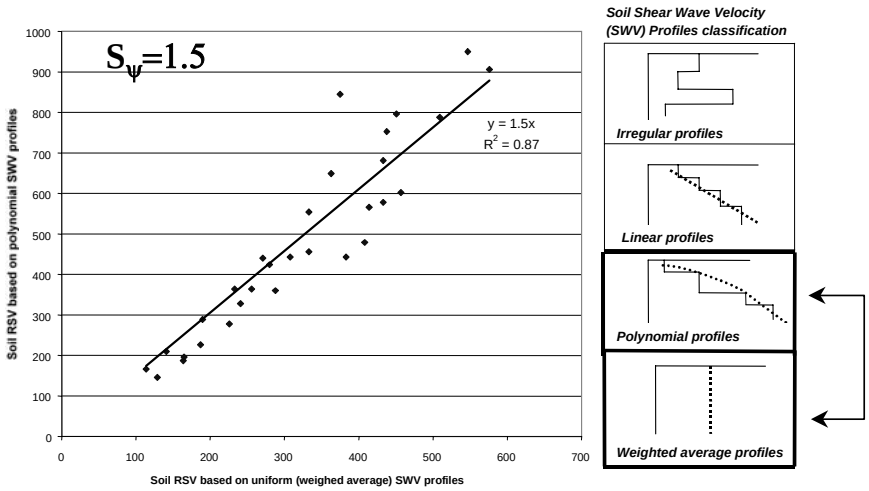

(c) Polynomial versus Uniform SWV profiles

Fig. 15 Soil shear wave velocity profile effects on the soil amplification factor (after Venkatesan (2004))

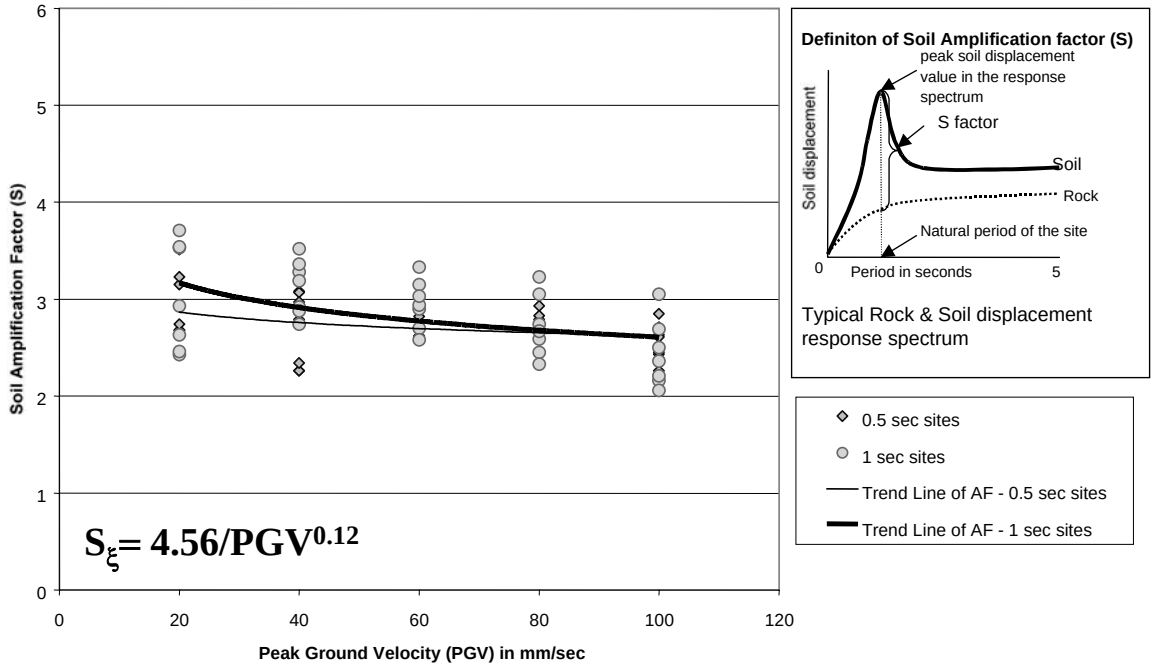

Fig. 16 Effects of intensity (hysteretic damping) (after Venkatesan (2004))

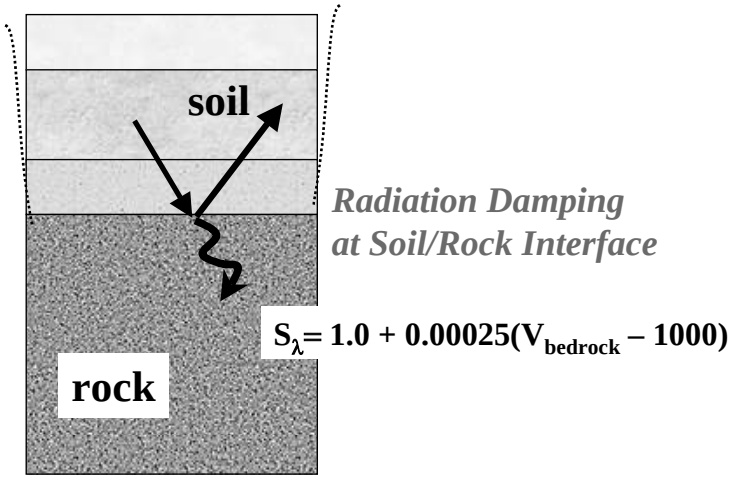

Fig. 17 Effects of radiation damping (after Venkatesan (2004))

In summary, the peak displacement demand on flexible soil in intraplate conditions is defined by Equations (17)-(18) (and shown diagrammatically in Figure 14):

$$RSD(\text{soil})_{\max} = S.RSV(\text{rock})_{\max}.\frac{T_s}{2\pi} \tag{17a}$$

$$RSD(\text{soil})_{\max} = S.RSD(\text{rock})_{\max} \tag{17b}$$

whichever is smaller.

$$S = S_\psi.S_\xi.S_\lambda \tag{18a}$$

where

S_ψ = 1.0 for soils possessing a uniform shear wave velocity profile (reference case),
S_ψ = 1.3 for irregular profiles typically found in practice, and
S_ψ = 1.4 and 1.5 for profiles having distinct "linear" and "polynomial" shapes respectively (18b)

$$S_\xi = 4.56/PGV^{0.12} \tag{18c}$$

where PGV (in units of mm) is at the bedrock surface and is in the range of 20-100 mm/sec,

and

$$S_\lambda = 1 + 0.00025\left(V_{\text{bedrock}} - 1000\right) \tag{18d}$$

$$0.9 \le S_\lambda \le 1.25$$

where V_{bedrock} is bedrock *SWV* in m/sec.

Note, the S_λ factor in the above formulation has been normalised to unity at the reference V_{bedrock} value of 1000 m/sec (expressions presented previously in Lam et al. (2001) and Lam and Wilson (2003) were normalised to unity at a higher V_{bedrock} value).

Significantly, the S factor computed from this study is considerably higher than that stipulated by current code models (e.g., IBC, 2000; Martin and Dobry, 1994) as shown in Venkatesan et al. (2003). Code based soil amplification factors are generally not represented fully by existing empirical models (e.g., Crouse and McGuire, 1996; Borcherdt, 1994), since they have typically been obtained by averaging response spectra for soil sites with a range of site periods (refer Figure 17 of Chandler et al. (2002a) for a detailed illustration). The effects of soil resonance have therefore been "smeared" through the averaging process, and are generally non-conservative for a given site.

The displacement demand behaviour associated with soil resonance is not always evident from a response spectrum because different response spectrum formats place different emphasis on the same spectral information (refer Figures 13(a)-13(d)). For example, the dominant peak in the *RSD* spectrum representing the highest displacement demand (Figure 13(d)) only appears as a minor peak in the *RSA* spectrum in which spectral peaks at lower periods are shown more prominently (Figure 13(a)). It should also be noted that resonance effects could be suppressed effectively by energy absorption in ductile systems along with hysteretic and radiation damping in the soil. Consequently, soil response models that have proven to be satisfactory in high seismic regions may not be best suited to applications in low-moderate seismic regions.

Overall, the bi-linear displacement spectrum construction, introduced in this section, represents a major paradigm shift in the way seismic demand is modelled on soil sites.

APPLICATION OF DISPLACEMENT MODEL

1. Displacement Demand of a Single-Degree-of-Freedom System

A notional 5% damping is normally assumed in the calculation of the displacement spectrum. Artificially increased "substitute" viscous damping to simulate inelastic behaviour has been proposed (Shibata and Sozen, 1976; Priestley, 1995). This approach in determining displacement demand has been found to provide reasonable results when the ductility demand is limited $(\text{i.e.}\,\mu \le 3)$, but may lead to non-conservative predictions with higher ductility demands (Miranda and Ruiz-Garcia, 2002). The notion of a 5% nominal damping for elastic behaviour is not theoretically correct and is a simplification. Equivalent damping has been studied in details by the authors (e.g., Edwards et al., 2003), but a rigorous treatment does not seem to be justified in an intraplate environment in view of the limited ductility in structures. At a ductility demand of $\mu = 2$, an equivalent damping ratio of about 15% is recommended by Priestley (1995) and 12% by Iwan and Gates (1979) assuming a "column-mechanism" behaviour. An assumption of 10% damping is not unreasonable for the assessment of the "life-safety" performance behaviour of structures characterised by such conditions. The well known expression (Equation (19)), originally developed by Newmark and Hall (1982) for determining the correcting factor for damping, has been found to be particularly applicable to conditions at resonance (Lam et al., 2001). This equation translates a 10% viscous damping into a damping factor ψ = 0.8:

$$\psi = \sqrt{\frac{7}{\xi + 2}} \tag{19}$$

where ξ is the equivalent damping in percentage.

As yielding of the structure can be represented by period-shift and increased damping, the displacement demand imposed on an inelastically responding system can be tracked by the elastic displacement response spectrum (refer Figure 18). Importantly, structures that have reached the peak displacement limit ($RSD_{\max}$) will experience "displacement-controlled" conditions in which the global response behaviour of the structure is insensitive to variations in the mass or stiffness of the structure. With displacement-controlled behaviour (Lam and Chandler, 2004), seismic performance could be assessed by simply comparing $RSD_{\max}$ against the displacement capacity of the structure.

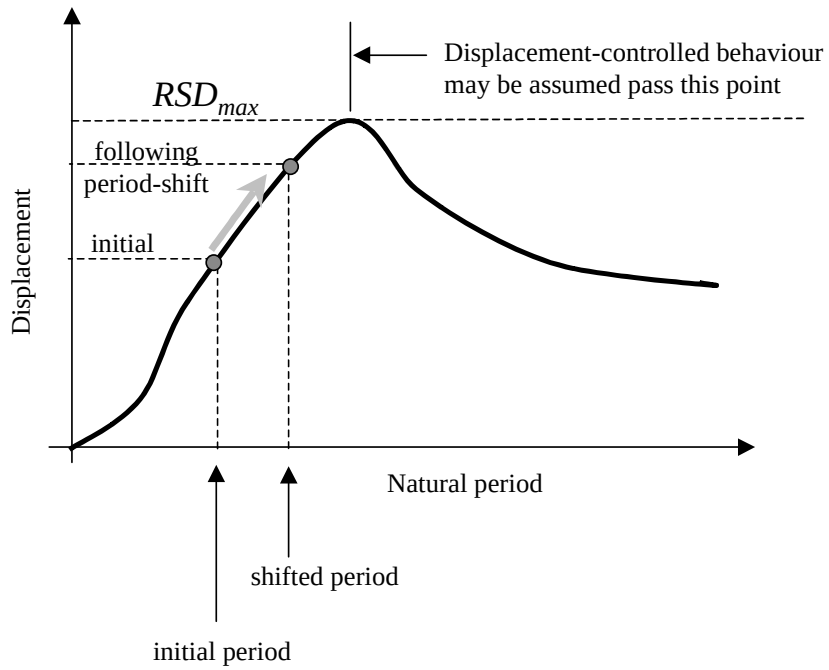

Fig. 18 Effect of period-shift on displacement demand

2. Case-Study No. 1: Seismic Assessment of a Soft-Storey Building

The force-displacement behaviour of a soft-storey building is illustrated in this section based on the case study of a real building in Australia (refer Figure 19(a)). The displacement of the soft-storey is contributed primarily by the deformation of the columns. Column deformation is made up of flexural deformation, shear deformation, yield penetration and end rotation. Flexural deformation could be estimated with good accuracy by integrating curvatures that have been calculated in accordance with representative stress-strain relationships of both concrete and steel (Watson et al., 1994), assuming plane section remaining plane.

Shear deformation is particularly significant with short columns possessing low shear-span to depth ratios. In this study, a truss analogy method developed for cracked concrete (Park and Paulay, 1975) was used to predict shear deformation assuming linear elastic behaviour of the concrete "struts" and the steel "ties". The accuracy of this model has yet to be verified by comparison with results from experiments in which shear deformation could be measured.

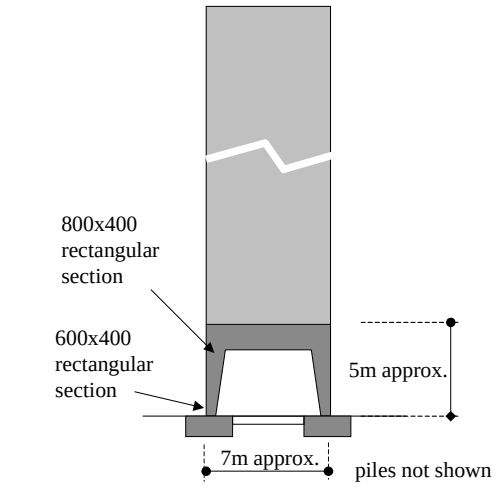

(a)

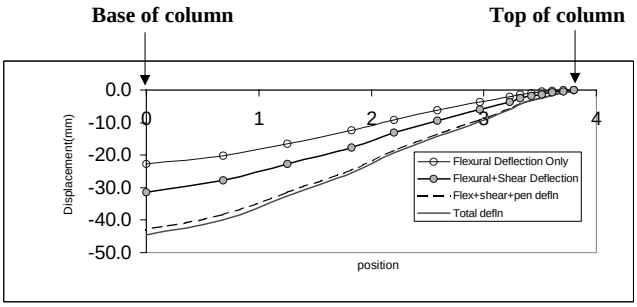

(b)

Fig. 19 Case study of a soft-storey building

The effects of yield penetration in the column longitudinal reinforcement at the anchorage to the foundation was calculated in accordance with the recommendations by Alsiwat and Saatcioglu (1992), which assumes uniform elastic bond stress and frictional bond stress in different sections along the development length of the reinforcement. Finally, end rotations of the column contributed mainly by the flexibility of the piled foundation and the connecting ground beams have been incorporated into the analysis.

The relative contributions from each of the deformation mechanisms to the total deformation of the column have been studied by pushover analysis using the example column shown in Figure 19(b). The displacement behaviour of the portal frame as a whole is also shown (refer Figure 19(c)).

Analysis results show that compressive stresses in the columns arising from the "push-pull" actions, associated with the application of the horizontal load, could be very significant. The initial axial load ratio of 0.15 under gravity loading could be increased to 0.3 as the estimated horizontal force is applied to the frame. Importantly, the stiffness properties of the column is very sensitive to the induced axial compression. Consequently, columns within the same portal frame possess very different stiffness properties.

The force-displacement relationship (defining the effective stiffness) of the individual columns are presented in Figure 19(b) along with that representing the portal frame as a whole (with and without taking into account P-Δ effects) as shown in Figure 19(c). Finally, the calculated displacement of the superstructure (which includes the effects of the tilting of the foundation) have been included in the analysis to obtain the "global" force-displacement relationship of the building (refer last item on the legend in Figure 19(c)).

The differential stiffness in the columns resulted in a very uneven sharing of the horizontal shear forces between the columns within the portal frame. In the presented case study of a 13-storey building, the more heavily loaded column (i.e. column subject to a higher compressive stress) attracted twice the shear force of a lightly loaded column. Such differential load-sharing between the columns is typically not

modelled by the average structural analysis packages that are currently used in practice. Thus, the seismically induced shear stress in columns in a soft-storey is often understated by conventional analyses.

The force-displacement relationship calculated for the portal frame (Figure 19(c)) was then used for the assembly of the force-displacement relationship for the entire building which is "star-shaped" in plan. The "performance point" was then determined by intercepting the calculated capacity curves of the building with the seismic demand curves predicted for a return period for 500 years as shown in Figure 19(d). It is noted that the seismic demand curves were developed from a pre-defined value of *PGV*, based on code recommendations (Wilson and Lam, 2003), in conjunction with a corner period T_2 of 1.5 sec (refer Sub-section 4 in the third section). This simple approach is distinguished from a more elaborate procedure in which design earthquake scenarios defined in terms of *M-R* combinations are identified. Thus, details of evaluating the individual component factors for substitution into Equation (2) have not been shown in this case study. A conservative 5% damping has also been assumed and hence no iteration was carried out in the calculation for the equivalent damping.

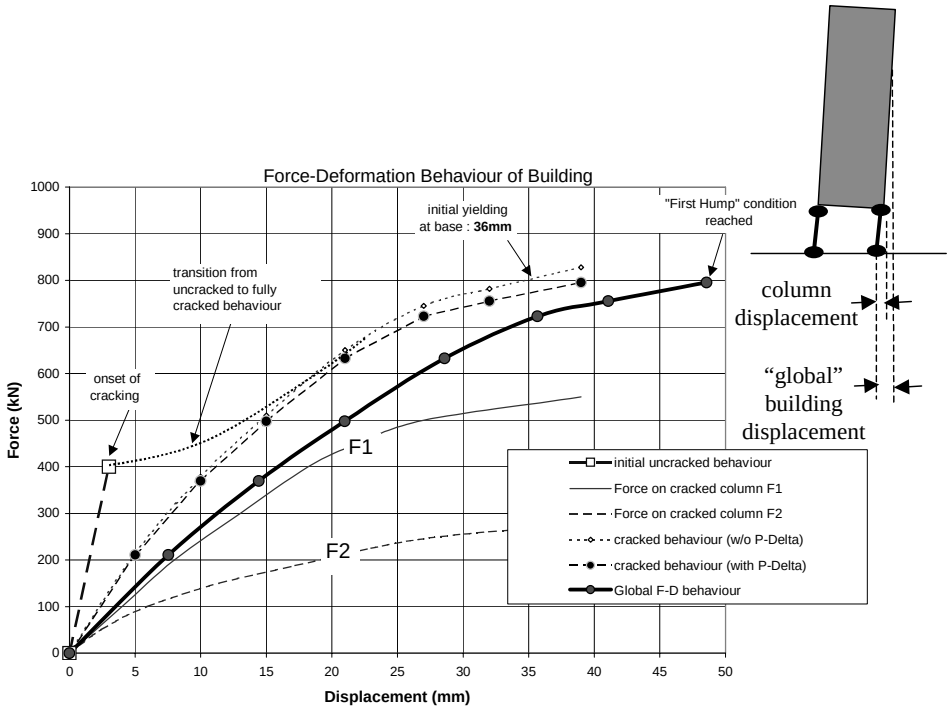

(c)

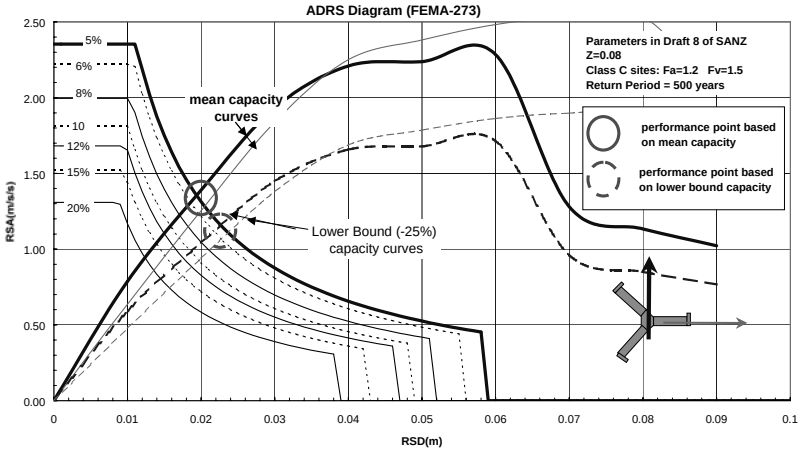

(d)

Fig. 19 Case study of a soft-storey building (continued)

3. Case-Study No. 2: Seismic Assessment of a Water Outlet Tower

The Outlet tower (Figure 20(a)) is a 71m tall reinforced concrete structure with an internal shaft approximately 8 m in diameter. The internal shaft is surrounded by 10 equally spaced radial fins for the lower 60 m of the tower which provide stability to the structure and increase the effective diameter to 18.2 m. The upper 11 m of the tower consists of an enclosed space for machinery and equipment. Bulkhead gates replace the internal shaft for the base 4.6 m of the Outlet tower to allow the passage of water into the tower. The maximum water level for the reservoir is assumed 52.3 m above the base.

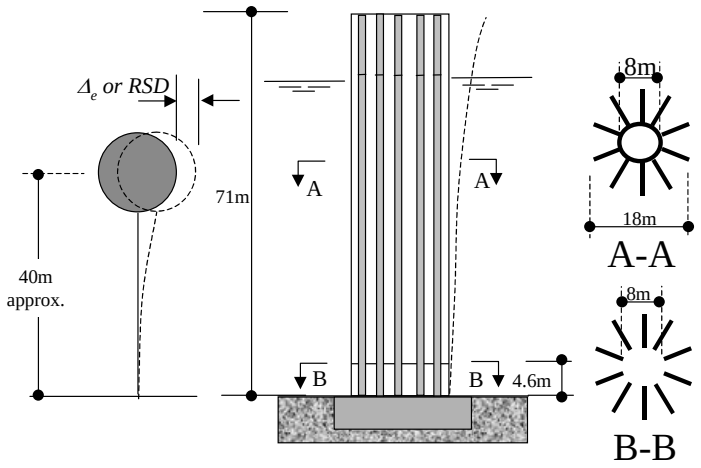

(a)

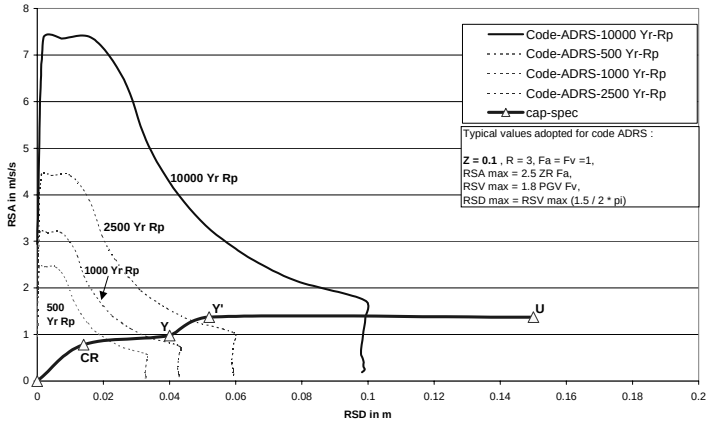

(b)

Fig. 20 Case study of a water outlet tower

The approximate 21,000 tonnes of seismic mass of the structure consists of:

- Structural concrete 8000 tonnes,
- Machinery and equipment 500 tonnes
- Hydrodynamic mass 12,500 tonnes

The Capacity Spectrum method was used to estimate the likely performance of the outlet tower at both the Operational Based Event (OBE) and Maximum Design Events (MDE). The Capacity Spectrum method involves comparing the seismic demand with the structural capacity in terms of an acceleration displacement response spectrum representation (ADRS format) as shown in Figure 20(b). The results, as plotted in the figure, clearly indicate that the tower is satisfactory for both the OBE and MDE events with displacement demands in the order of 40 mm and 100 mm respectively. The analyses suggest that the tower would crack and the reinforcement at the outer diameter of the tower fins may almost yield at the OBE. It is expected that the tower would remain operational at the OBE with these small drifts of around

0.1%. The tower has the capacity to displace at least 150 mm under ultimate conditions which is well in excess of the 100 mm demand associated with the MDE event. It is expected that the reinforcement would yield extensively at the MDE with some minor damage at the associated 0.20-0.25% drift. The seismic demand curves were developed in a manner similar to Case Study No. 1.

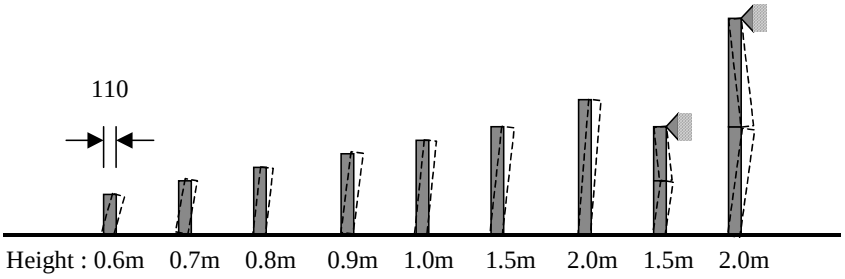

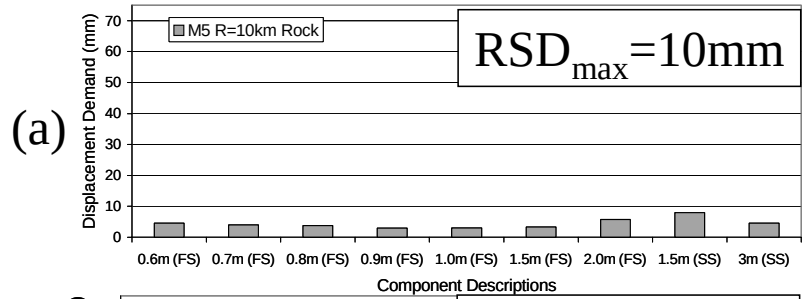

Figure 5a

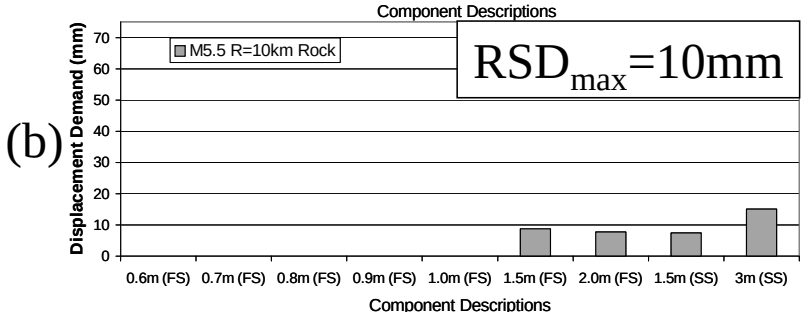

Figure 5b

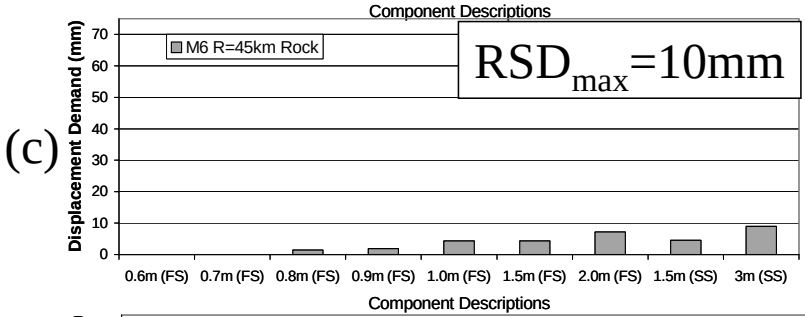

Figure 5c

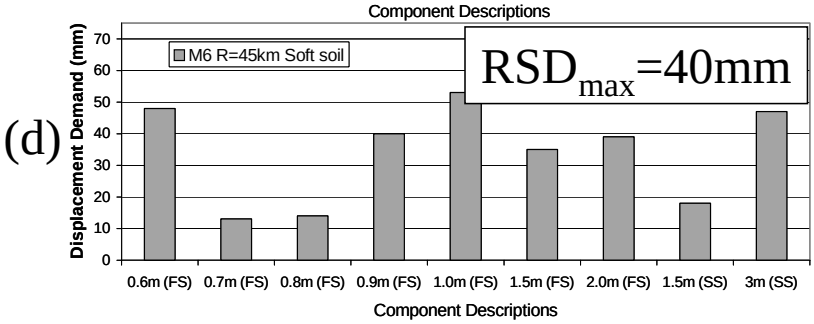

Figure 5d

Fig. 21 Displacement-controlled behaviour of rigid objects

4. Case-Study No. 3: Seismic Assessment of Rigid Objects

Displacement-controlled behaviour has been demonstrated from the analysis of rigid free-standing (FS) components which exhibit significant period-shift during a rocking response. Such FS components include parapet walls, unrestrained equipment and other building contents. Widespread failure (e.g. overturning) of these components has resulted in casualties and very high economic losses during many earthquakes around the world including low-moderate seismic regions (e.g. 1989 Newcastle earthquake). Being rigid, the components possess very low initial natural periods. However, their force-displacement behaviour is characterized by significant *P-Δ* effects causing a rapid decrease in resistance to overturning with increasing displacement.

To illustrate the rocking phenomenon of walls, seven FS objects with heights varying between 0.6 m and 2.0 m, and two simply-supported (SS) block models with initial periods of approximately 0.5 sec have been subject to varying degrees of earthquake excitations. All walls were assumed single-leaf URM, of thickness equal to 110 mm. The displacement capacity of the wall is defined as the maximum displacement that will cause the wall to overturn. The displacement capacity for a 110 mm thick wall is 110 mm at the top of the wall and 75 mm (two-thirds of wall thickness) at the effective wall height.

Assuming displacement-controlled behaviour, the walls are considered safe from overturning provided the 75 mm displacement capacity limit is not exceeded by the peak displacement demand ($RSD_{\max}$) of the applied excitation. To test this assumption, each of the models shown on the top of Figure 21 was subject to non-linear time-history analysis (THA) using a selection of ground motions with $RSD_{\max}$ ranging between 10 mm and 40 mm. Accuracies of the computer program, which conducted the THA, have been verified by comparison with shaking-table experiments (Lam et al., 2003b). The maximum displacement demands calculated from the analyses have been plotted in Figures 21(a)-21(d) and were generally in good agreement with the $RSD_{\max}$ of the respective earthquake records. Overturning was predicted by the particular analyses that were based on records with $RSD_{\max}$ exceeding 75 mm (not shown in Figure 21). This simple example demonstrates the effectiveness of a displacement-based (DB) procedure, which was in turn confirmed through time-history analyses.

5. Extension of the Displacement Model

Research is currently underway to extend the displacement model to account for higher modes effects, torsional effects, and to develop displacement floor spectra for predicting the seismic performance of unrestrained components in multi-storey buildings. Each of these topics is a subject in its own right and hence only an overview of the proposed approach is outlined herein. The objective is to promote further research attention into these important aspects of displacement modelling. These effects have not been discussed in the case studies but could be a significant issue in certain practical applications.

Maximum dynamic drift in the building which includes contributions from the higher vibration modes can be estimated from the displacement model introduced in this paper (i.e. Equations (1)-(2) and the associated factors) in conjunction with the participation factor and the λ_1 and λ_2 factors defined in Figure 22. The displacement demand predicted for the equivalent single-degree-of-freedom (SDOF) system corresponds to the displacement (Δ_e) at the effective height which is typically 0.6-0.7 times the full height of the building. Interestingly, Δ_e can be taken to be equal to $RSD_{\max}$ when (conservatively) assuming displacement-controlled behaviour.

An approximation to the deflection profile of the building can be obtained from a quasi-static analysis using a distributed force which varies linearly from zero intensity at the base to maximum intensity at roof level as shown in Figure 22(a). The displacement demand at the roof level is then the product of Δ_e and the participation factor (PF) associated with the assumed deflection profile. The average drift angle (θ_{avg}) is accordingly the roof displacement divided by the height of the building. The maximum drift angle is, by definition, equal to $\lambda_1\theta_{\text{avg}}$, where λ_1 is a correction factor for the actual deflection shape and may be taken to be equal to 2 according to recommendations by Paulay and Priestley (1992) and Priestley (1995) for elastically responding frame buildings based on the shape of a parabola. The recommended higher mode (dynamic) factor of λ_2 = 1.3-1.8 (Paulay and Priestley, 1992) is consistent with preliminary findings by the authors. Systematic studies to correlate the PF, λ_1 and λ_2 factors with building parameters in

intraplate regions are currently underway. Preliminary findings from collaborative research were reported by Chandler et al. (2002b).

The direct DB approach demonstrated herein for predicting maximum displacement and drifts in a building is distinguished from the conventional force-based (FB) approach of first estimating the seismic base shear, then distributing the shear force along the height of the building, and then finally dividing the storey-shear by the estimated storey-stiffness.

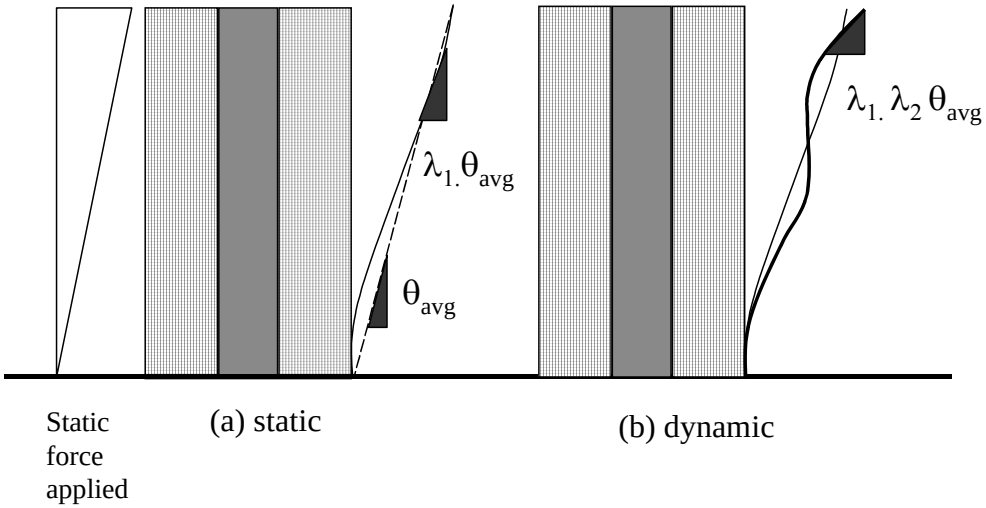

Fig. 22 Modelling for inter-storey drift

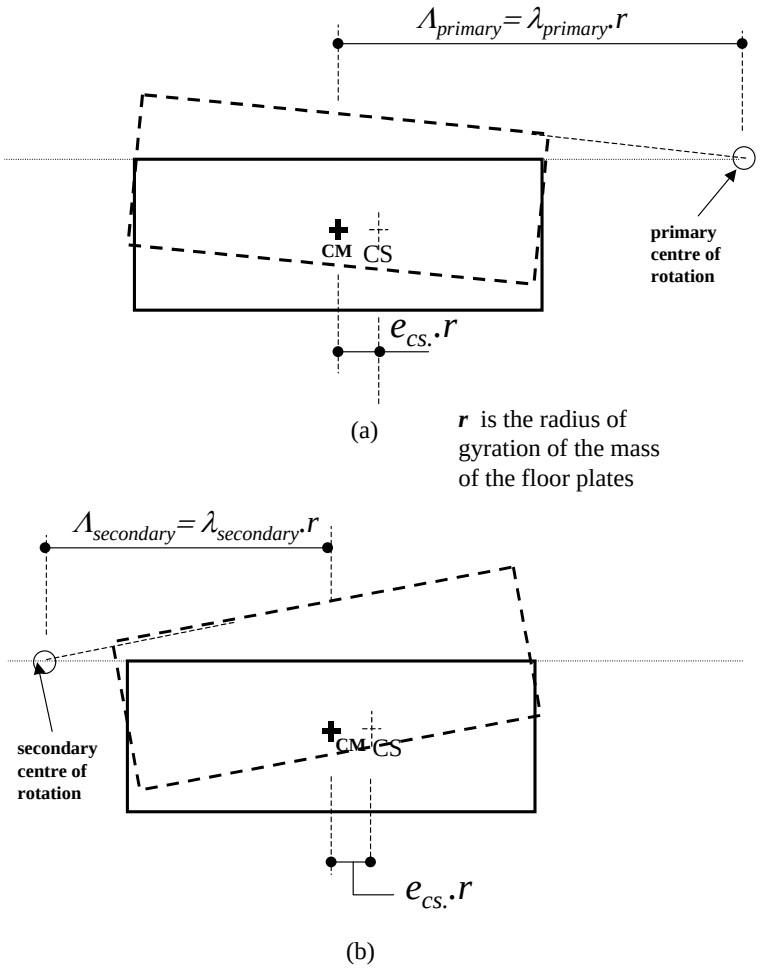

Fig. 23 Modelling of displacement amplification by torsion

The concept of de-coupling displacement calculations from the consideration of force and stiffnesses can be extended to the analysis of seismically induced torsional effects in buildings with horizontal irregularities. Torsional effects characterised in terms of displacement are in better alignment with performance-based principles than conventional parameters such as design eccentricity, strength demand or ductility demand. A new format of representing torsional amplification of displacement by locating the instantaneous centres of rotation has been developed. The displacement at different locations in the building can be determined for any given centre of rotation and displacement at the centre of mass (refer Figure 23). This new modelling approach has been demonstrated in the seismic assessment of a 16-storey wall-frame building in Singapore (Balendra et al., 2004). Results on a recent parametric studies on the behaviour of the $\lambda_{primary}$ and $\lambda_{secondary}$ parameters have been reported by Lumantarna et al. (2003).

The concept of modelling potential damage to non-structural components in a building by considering the combined predictions for the maximum floor response spectra in terms of acceleration (RSA_{maxf}), velocity (RSV_{maxf}), and displacement (RSD_{maxf}) demand was first introduced in Lam and Gad (2002) (the notations used in representing ground shaking and floor shaking are similar except for the use of the additional "f" subscript in the latter). These three response spectral terms can be conveniently used to construct a tri-linear velocity spectrum model in the tri-partite format (Lam and Gad, 2002). It is shown in Figure 24 that certain damage scenarios related to the failure of ceiling components and building contents risking overturning and sliding are better represented by the displacement demand of the building floor as opposed to the so called peak floor acceleration (PFA). Clearly, the conventional code approach of using design PFA to characterise the seismic demand on non-structural components is useful for evaluating the force demand on fully restrained components but provides very limited information on the potential impact velocities and instabilities for other components. The predicted seismic demands (RSA_{maxf}, RSV_{maxf} and RSD_{maxf}) on a building floor requires combining information obtained from both the acceleration and displacement floor spectra. Displacement floor spectra have been developed for buildings of different heights and at different levels up the height of the building in a recent collaborative study (Al Abadi et al., 2004).

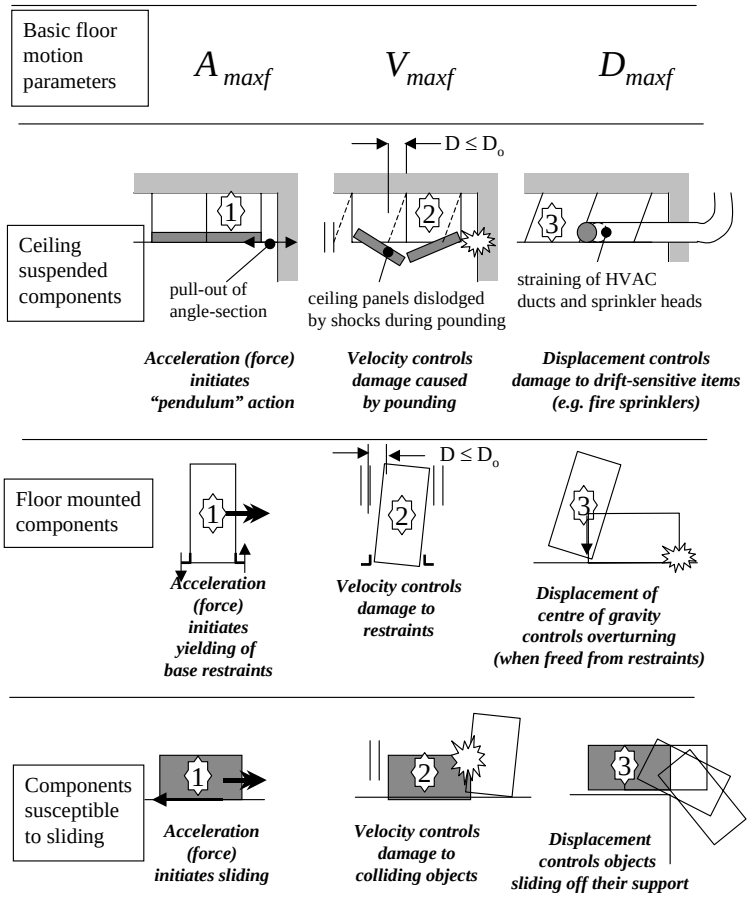

Fig. 24 Displacement behaviour of non-structural components

SUMMARY OF RECOMMENDATIONS AND CONCLUSIONS

This paper presents the case for a displacement-based approach for the seismic design and performance assessment of structures in intraplate regions. A Component Attenuation Model (CAM) is presented for predicting the seismic displacement demand of intraplate earthquakes as functions of the magnitude-distance (*M*-*R*) combinations along with numerous geophysical and geotechnical parameters. The generic expression of Equation (2) for predicting the peak displacement demand or peak velocity demand ($RSD_{\max}$ or $RSV_{\max}$ respectively), which jointly define the displacement response spectrum, is presented as the product of numerous component factors that represent various source, path and site effects as summarised in Table 2.

Table 2: Summary of Component Attenuation Model (CAM) for Displacement Predictions

Component Factor	Expressions for $RSD_{\max}$ (mm)	Expressions for $RSV_{\max}$ (mm/sec)	Reference to Text
α	10^{M-5} [Equation (11)]	$70\{0.35+0.65(M-5)\}^{1.8}$ [Equation (12)]	Source factor
γ	1.0(min.)-1.6(max.) [Equation (13)]	1.0(min.)-2.0(max) [Equation (13)]	Crustal factor
G	$30/R$ [Equation (14a)] for near field Figure 10(a) for far field	$30/R$ [Equation (14a)] for near field Figure 10(a) for far field	Geometrical factor
β	$(30/R)^{0.003R}$ [Equation (14b)] for near field; Figure 10(b) for far field	$(30/R)^{0.005R}$ [Equation (14b)] for near field; Chandler and Lam (2004) for far-field	Anelastic attenuation factor
S	-	Equation (18)	Site factor
ψ	0.8 assuming 10% damping or Equation (19)	0.8 assuming 10% damping or Equation (19)	Damping factor

A worked example demonstrating the use of the CAM expressions summarised in Table 2 to predict the displacement demand for a pre-defined earthquake scenario is shown in Appendix A.

In situations where the design earthquake scenarios defined by *M*-*R* combinations are not given, the displacement response spectrum could be constructed in accordance with the predicted value of $RSV_{\max}$ parameter (which may be taken as 1.8 times the design peak ground velocity) along with the assumed corner period, T_2 (which can be estimated using Equation (16)). In modelling distant earthquakes, the displacement response spectrum could be constructed in accordance with the predicted value of $RSD_{\max}$ along with the assumed corner period in a so called "reverse procedure".

The displacement response spectrum can be presented in the alternative ADRS format for determination of the "performance points" in a capacity spectrum procedure as demonstrated in the case studies of a soft-storey building and an water outlet tower. Displacement controlled behaviour was further demonstrated by stability analyses of rigid objects. The proposed displacement model could be further developed into more sophisticated models that incorporate effects of the higher modes and dynamic torsion, or provide estimates for displacement floor spectra.

ACKNOWLEDGEMENTS

The displacement model described in this paper forms part of the outcome of major strategic research programs to address seismic risks in Australia. Research has been undertaken at the University of Melbourne since 1993, and has received continuous funding from the Australian Commonwealth government. Invaluable research contributions over the years by Prof. Adrian Chandler of Hong Kong University (with funding support from the Research Grants Council of Hong Kong) is specifically acknowledged. Acknowledgement is also given to continuous support and input by A/Prof. Mike Griffith of The University of Adelaide, Dr Martin Kwong of Scott Wilson Consulting Engineers, A/Prof Balendra of The National University of Singapore, Prof. Yuxian Hu of the China Seismological Bureau and A/Prof. Pennung Warnitchai of Asian Institute of Technology in related collaborative studies.

APPENDIX A: EXAMPLE ON DISPLACEMENT PREDICTIONS USING THE COMPONENT ATTENUATION MODEL (CAM)

Input Parameters:

Moment Magnitude (M) = 5.6 (e.g. 1989 Newcastle earthquake, New South Wales, Australia)

Hypocentral Distance (R) = 15 km; shallow earthquake.

Young geological formation with high energy absorption properties which is consistent with conditions of the Sydney basin (*kappa* = 0.05 assumed).

Q_o = 200 (note, the effect of Q on the attenuation of near-field earthquakes is not significant)

Crustal depth D = 30 km (irrelevant to the attenuation of near-field earthquakes)

V_{bedrock} is in the order of 800 m/sec

Site natural period (T_s) = 0.6 sec; shape of soil shear wave velocity profile uncertain

The value of $RSD_{\max}$ and $RSV_{\max}$ for average rock sites based on the product of the component factors $\alpha.\gamma.G.\beta$ as listed in Table A.1 below is accordingly:

$RSD_{\max}$ (rock) = 4 mm (1.6) (2.0) (1.03) = <u>13 mm</u>

$RSV_{\max}$ (rock) = 40 mm/sec (1.6) (2.0) (1.05) = <u>134 mm/sec</u>

PGV(rock) = 134/2 = <u>65 mm/sec</u> [Equation (15)]

MMI is about VI-VII on rock sites according to the expression of Newmark and Rosenblueth (1971)

In calculating the S factor using Equation (18):

S_ψ = 1.3-1.5 [Equation (18b)], S_ξ = 2.8 [Equation (18c)] and S_λ = 0.95 [Equation (18d)]

S = 3.5-4.0 and hence

$RSV_{\max}$ (soil)=$S \times$ $RSV_{\max}$ (rock)= <u>470-540 mm/sec</u>

$RSD_{\max}$ (soil)=$S \times$ $RSV_{\max}$ (rock).$T_s/2\pi$ = 45-50 mm [Equation (17a)]

$RSD_{\max}$ (soil)=$S \times$ $RSD_{\max}$ (rock) = 45-50 mm [Equation (17b)]

whichever is smaller.

$RSD_{\max}$ (soil) = <u>45-50 mm</u>

Table A.1: Substitution of Input Parameters into CAM

Component Factor	Expressions for $RSD_{\max}$ (mm)	Expressions for $RSV_{\max}$ (mm/sec)	Reference to Text
α	4mm [Equation (11)]	40 mm/sec [Equation (12)]	Source factor [Third section, Sub-section 1]
γ	1.6 [Equation (13)]	1.6 [Equation (13)]	Crustal factor [Third section, Sub-section 2]
G	2.0 [Equation (14a)]	2.0 [Equation (14a)]	Geometrical factor [Third section, Sub-section 3]
β	1.03 [Equation (14b)]	1.05 [Equation (14b)]	Anelastic attenuation factor [Third section, Sub-section 3]
S	-	3.5-4.0[Equation (18)]	Site factor [Fourth section]
ψ	1.0 (5% damping) 0.8 (10% damping)	1.0 (5% damping) 0.8 (10% damping)	Damping factor [Fifth section, Sub-section 1]

The displacement demand at the centre of inertia (Δ_e) of a single-degree-of-freedom system founded on the soil surface is estimated at 45-50 mm assuming 5% damping, according to the calculations.

For an unreinforced masonry (URM) wall, experiencing rocking motion, for example, the maximum displacement of the wall is about 70-75 mm (being $1.5\Delta_e$), which is some 30-40% from the ultimate limit of 110 mm (i.e. the displacement limit for overturning of a single-leaf wall). Refer Doherty et al. (2002) for details of this assessment approach. Walls at the upper levels of a building is subject to an even higher risk of collapsing due to the displacement amplification by the building (not taken into account by CAM).

The *MMI* = VI-VII, predicted on rock sites in this example, is consistent with the report on the 1989 Newcastle earthquake (Melchers, 1990). The high overturning risk, predicted for URM walls on soil sites, is also very consistent with the report of widespread collapse of URM walls in the earthquake.

REFERENCES

1. Abercrombie, R.E. (1997). "Near-Surface Attenuation and Site Effects from Comparison of Surface and Deep Borehole Recordings", Bull. Seism. Soc. Am., Vol. 87, pp. 731-744.
2. Abrahamson, N.A. and Silva, W.J. (1997). "Empirical Response Spectral Attenuation Relations for Shallow Crustal Earthquakes", Seismological Research Letters, Vol. 68, No. 1, pp. 94-127.
3. Al Abadi, H.A., Lam, N.T.K., Gad, E.G. and Chandler, A.M. (2004). "Earthquake Floor Spectra for Unrestrained Building Components", International Journal of Structural Stability and Dynamics (in press).
4. Alsiwat, M. and Saatcioglu, M. (1992). "Reinforcement Anchorage Slip under Monotonic Loading", Journal of Structural Engineering, ASCE, Vol. 118, No. 9, pp. 2421-2437.
5. Anagnostopoulos, S.A., Haviland, R.W. and Biggs, J.M. (1978). "Use of Inelastic Spectra in Aseismic Design", Journal of the Structural Division, ASCE, Vol. 104, No. ST1, pp. 95-109.
6. Anderson, J.G. and Hough, S.E. (1984). "A Model for the Shape of the Fourier Amplitude Spectrum of Acceleration at High Frequencies", Bull. Seism. Soc. Am., Vol. 74, No. 5, pp. 1969-1993.
7. AS1170.4 (1993). "Minimum Design Loads on Structures: Part 4 - Earthquake Loads", Standards Association of Australia, Australia.
8. Asten, M. and Dhu, T. (2002). "Enhanced Interpretation of Microtremor Spectral Ratios in Seismic Hazard Zonation Using Multimode Rayleigh-Wave Particle Motion Computations", Proc. Aus. Earthquake Eng. Soc. Conf., Adelaide, Australia, Paper No. 8.
9. Asten, M., Lam, N.T.K., Gibson, G. and Wilson, J.L. (2002). "Microtremor Survey Design Optimized for Application to Site Amplification and Resonance Modeling", Proc. Aus. Earthquake Eng. Soc. Conf., Adelaide, Australia, Paper No. 7.
10. Asten, M. (2003). Personal communications with the authors.
11. ATC (1996). "Seismic Evaluation and Retrofit of Concrete Buildings", Report ATC-40, Applied Technology Council, Redwood City, CA, U.S.A.
12. Atkinson, G.M. (1993). "Earthquake Source Spectra in Eastern North America", Bull. Seism. Soc. Am., Vol. 83, pp. 1778-1798.
13. Atkinson, G.M. and Boore, D.M. (1995). "New Ground Motion Relations for Eastern North America", Bull. Seism. Soc. Am., Vol. 85, No. 1, pp. 17-30.
14. Atkinson, G.M. and Boore, D.M. (1998). "Evaluation of Models for Earthquake Source Spectra in Eastern North America", Bull. Seism. Soc. Am., Vol. 88, No. 4, pp. 917-937.
15. Atkinson, G.M. and Mereu, R.F. (1992). "The Shape of Ground Motion Attenuation Curves in Southeastern Canada", Bull. Seism. Soc. Am., Vol. 82, No. 5, pp. 2014-2031.
16. Atkinson, G.M. and Silva, W. (1997). "An Empirical Study of Earthquake Source Spectra for Californian Earthquakes", Bull. Seism. Soc. Am., Vol. 87, pp. 97-113.
17. Atkinson, G.M. and Silva, W. (2000). "Stochastic Modeling of Californian Ground Motions", Bull. Seism. Soc. Am., Vol. 90, pp. 255-274.
18. Balendra, T., Lam, N.T.K., Perry, M., Lumantarna, E. and Wilson, J.L. (2004). "Simplified Displacement Demand Prediction of Tall Asymmetric Buildings Subjected to Long Distance Earthquakes", Engineering Structures (tentatively accepted).

19. Balendra, T., Lam, N.T.K., Wilson, J.L. and Kong, K.H. (2002). "Analysis of Long-Distance Earthquake Tremors and Base Shear Demand for Buildings in Singapore", Engineering Structures, Vol. 2, pp. 99-108.
20. Beresnev, I.A. and Atkinson, G.M. (1997). "Modelling Finite-Fault Radiation from the ω^n Spectrum", Bull. Seism. Soc. Am., Vol. 87, pp. 67-84.
21. Bommer, J.J. and Elnashai, A.S. (1999). "Displacement Spectra for Seismic Design", Journal of Earthquake Engineering, Vol. 3, No. 1, pp. 1-32.
22. Boore, D.M. (1983). "Stochastic Simulation of High-Frequency Ground Motions Based on Seismological Model of the Radiated Spectra", Bull. Seism. Soc. Am., Vol. 73, No. 6, pp. 1865-1894.
23. Boore, D.M. and Joyner, W.B. (1997). "Site Amplifications for Generic Rock Sites", Bull. Seism. Soc. Am., Vol. 87, No. 2, pp. 327-341.
24. Borcherdt, R.D. (1994). "Estimates of Site-Dependent Response Spectra for Design (Methodology and Justification)", Earthquake Spectra, Vol. 10, pp. 617-653.
25. Chandler, A.M. (2003). personal communications on materials generated from collaborative research with The University of Hong Kong and yet to be published.
26. Chandler, A.M. and Lam, N.T.K. (2002). "Intensity Attenuation Relationship for the South China Region and Comparison with the Component Attenuation Model", Journal of Asian Earth Sciences, Vol. 20, pp. 775-790.
27. Chandler, A.M. and Lam, N.T.K. (2004). "An Attenuation Model for Distant Earthquakes", Earthquake Engineering and Structural Dynamics, Vol. 33, No. 2, pp. 183-210.
28. Chandler, A.M., Lam, N.T.K. and Sheikh, M.N. (2002a). "Response Spectrum Predictions for Potential Near-Field and Far-Field Earthquakes Affecting Hong Kong: Soil Sites", Soil Dynamics and Earthquake Engineering, Vol. 22, pp. 419-440.
29. Chandler, A.M., Su, R.K.L. and Sheikh, M.N. (2002b). "Drift-Based Seismic Assessment in Hong Kong", Proceedings of International Conference on Advances and New Challenges in Earthquake Engineering Research, Harbin and Hong Kong, China.
30. Crouse, C.B. and McGuire, J.W. (1996). "Site Response Studies for Purpose of Revising NEHRP Seismic Provisions", Earthquake Spectra, Vol. 12, No. 3, pp. 407-439.
31. Dahle, A., Bungum, H. and Kvamme, L.B. (1990). "Attenuation Models Inferred from Intraplate Earthquake Recordings", Earthquake Engineering and Structural Dynamics, Vol. 19, pp. 1125-1141.
32. Dickenson, S.E., Seed, R.B., Lysmer, J. and Mok, C.M. (1991). "Response of Soft Soils during the 1989 Loma Prieta Earthquake and Implications for Seismic Design Criteria", Proceedings of 4th Pacific Conference on Earthquake Engineering, Auckland, New Zealand, Vol. 3, pp. 191-204.
33. Doherty, K., Griffith, M., Lam, N.T.K. and Wilson, J.L. (2002). "Displacement-Based Analysis for Out-of-Plane Bending of Seismically Loaded Unreinforced Masonry Walls", Earthquake Engineering and Structural Dynamics, Vol. 31, No. 4, pp. 833-850.
34. Dowrick, D.J., Gibson, G. and McCue, K. (1995). "Seismic Hazard in Australia and New Zealand", Bulletin of the New Zealand National Society for Earthquake Engineering, Vol. 28, No. 4, pp. 279-287.
35. Edwards, M., Wilson, J.L. and Lam, N.T.K. (2003). "Seismic Displacement Response Predictions Using a Calibrated Substitute-Structure Approach", Proceedings of 6th Pacific Conference on Earthquake Engineering, University of Canterbury, Christchurch, New Zealand, Paper No. 110.
36. Freeman, S.A. (1998). "Development and Use of Capacity Spectrum Method", Proceedings of 6th US National Conference on Earthquake Engineering, Seattle, U.S.A.
37. Gaull, B.A., Michael-Leiba, M.O. and Rynn, J.M.W. (1990). "Probabilistic Earthquake Risk Maps of Australia", Australian Journal of Earth Sciences, Vol. 37, pp. 169-187.
38. Gibson, G., Wesson, V. and Jones, T. (1995). "Strong Motion from Shallow Intraplate Earthquakes", Proceedings of Pacific Conference on Earthquake Engineering, Vol. 2, pp. 185-193.
39. IBC (2000). "International Building Code", International Code Council, U.S.A.

40. Idriss, I.M. and Sun, J.I. (1991). "User's Manual for SHAKE-91", National Institute of Standards and Technology, Maryland, U.S.A. and Department of Civil and Environmental Engineering, University of California, Davis, U.S.A.
41. Iwan, W.D. and Gates, N.C. (1979). "Estimating Earthquake Response of Simple Hysteretic Structures", Journal of Engineering Mechanics Division, ASCE, Vol. 105, pp. 391-405.
42. Kanamori, H. (1993). "Magnitude Scale and Quantification of Earthquakes", Tectonophysics, Vol. 83, pp. 185-1999.
43. Kwong, M.H.C., Ng, H.K., Lam, N.T.K. and Chandler, A.M. (2000). "Motion Induced by Distant Earthquakes: The Practitioners' Perspective", Proceedings of the International Conference on Advances in Structural Dynamics, pp. 201-208.
44. Lai, S.S. and Biggs, J.M. (1980). "Inelastic Response Spectra for Aseismic Building Design", Journal of the Structural Division, ASCE, Vol. 106, No. ST1, pp. 1295-1310.
45. Lam, N.T.K., Wilson, J.L. and Hutchinson, G.L. (1998). "The Ductility Reduction Factor in the Seismic Design of Buildings", Earthquake Engineering and Structural Dynamics, Vol. 27, pp. 749-769.
46. Lam, N.T.K. and Wilson, J.L. (1999). "Estimation of the Site Natural Period from Borehole Records", Australian Journal of Structural Engineering, Vol. SE1, No. 3, pp. 179-199.
47. Lam, N.T.K., Wilson, J.L., Chandler, A.M. and Hutchinson, G.L. (2000a). "Response Spectral Relationships for Rock Sites Derived from the Component Attenuation Model", Earthquake Engineering and Structural Dynamics, Vol. 29, pp. 1457-1489.
48. Lam, N.T.K., Wilson, J.L., Chandler, A.M. and Hutchinson, G.L. (2000b). "Response Spectrum Modelling for Rock Sites in Low and Moderate Seismicity Regions Combining Velocity, Displacement and Acceleration Predictions", Earthquake Engineering and Structural Dynamics, Vol. 29, pp. 1491-1525.
49. Lam, N.T.K., Wilson, J.L. and Hutchinson, G.L. (2000c). "The Modelling of Intraplate Seismic Hazard Based on Displacement", Proceedings of 12th World Conference on Earthquake Engineering, Auckland, New Zealand, Paper No. 1933 (OS1-T4).
50. Lam, N.T.K., Wilson, J.L. and Hutchinson, G.L. (2000d). "Generation of Synthetic Earthquake Accelerograms Using Seismological Modeling: A Review", Journal of Earthquake Engineering, Vol. 4, No. 3, pp. 321-354.
51. Lam, N.T.K., Wilson, J.L. and Chandler, A.M. (2001). "Seismic Displacement Response Spectrum Estimated from the Frame Analogy Soil Amplification Model", Engineering Structures, Vol. 23, No. 11, pp. 1437-1452.
52. Lam, N.T.K., Chandler, A.M., Wilson, J.L. and Hutchinson, G.L. (2002). "The Prediction of Displacement and Velocity Demand of Long Distance Earthquakes", Proceedings of 12th European Conference on Earthquake Engineering, London, U.K., Paper No. 550.
53. Lam, N.T.K. and Gad, E. (2002). "An Innovative Approach to the Seismic Assessment of Non-structural Components in Buildings", Proceedings of the Australian Earthquake Engineering Society Annual Seminar, Adelaide, Australia.
54. Lam, N.T.K. and Wilson, J.L. (2003). "The Component Attenuation Model for Low and Moderate Seismic Regions", Proceedings of the 2003 Pacific Conference on Earthquake Engineering, Christchurch, New Zealand, Paper No. 99.
55. Lam, N.T.K., Sinadinovski, C., Koo, R.C.K. and Wilson, J.L. (2003a). "Peak Ground Velocity Modelling for Australian Earthquakes", International Journal of Seismology and Earthquake Engineering, Vol. 5, No. 2, pp. 11-22.
56. Lam, N.T.K., Griffith, M.C., Wilson, J.L. and Doherty, K. (2003b). "Time-History Analysis of URM Walls in Out-of-Plane Flexure", Engineering Structures, Vol. 25, pp. 743-754.
57. Lam, N.T.K. and Chandler, A.M. (2004). "Peak Displacement Demand Modelling for Small and Moderate Intraplate Earthquakes", Earthquake Engineering and Structural Dynamics (tentatively accepted).

58. Lumantarna, E., Lam, N.T.K. and Wilson, J.L. (2003). "A Displacement Approach to the Analysis for Seismically Induced Torsion in Buildings", Proceedings of the Australian Earthquake Engineering Society Annual Conference, Australia, Paper No. 15.
59. Mahin, S.A. and Lin, J. (1983). "Construction of Inelastic Response Spectra for Single-Degree-of-Freedom Systems (Computer Program and Applications)", Report UCB/EERC-83/17.
60. Martin, G.R. and Dobry, R. (1994). "Earthquake Site Response and Seismic Code Provisions", NCEER Bulletin, Vol. 8, No. 4, pp. 1-6.
61. Melchers, R.E. (1990). "Newcastle Earthquake Study", The Institution of Engineers, Australia.
62. Miranda, E. (1993). "Evaluation of Site-Dependent Inelastic Seismic Design Spectra", Journal of Structural Engineering, ASCE, Vol. 119, No. 5, pp. 1319-1338.
63. Miranda, E. and Ruiz-Garcia, J. (2002). "Evaluation of Approximate Methods to Estimate Maximum Inelastic Displacement Demands", Earthquake Engineering and Structural Dynamics, Vol. 31, pp. 539-560.
64. Newmark, N.M. and Hall, W.J. (1982). "Earthquake Spectra and Design", EERI Monograph, Earthquake Engineering Research Institute, California, U.S.A.
65. Newmark, N.M. and Rosenblueth, E. (1971). "Fundamentals of Earthquake Engineering", Prentice-Hall, New Jersey, U.S.A.
66. NZ4203 (1992). "Code of Practice for General Structural Design and Design Loadings for Buildings", New Zealand Standards, New Zealand.
67. Park, R. and Paulay, T. (1975). "Reinforced Concrete Structures", Wiley, U.S.A.
68. Paulay, T. and Priestley, M.J.N. (1992). "Seismic Design of Reinforced Concrete and Masonry Buildings", Wiley Interscience, New York, U.S.A.
69. Park, R. (1997). "A Static Force-Based Procedure for the Seismic Assessment of Existing Reinforced Concrete Moment Resisting Frames", Bulletin of New Zealand National Society for Earthquake Engineering, Vol. 30, No. 3, pp. 213-226.
70. Priestley, M.J.N. (1993). "Myths and Fallacies in Earthquake Engineering – Conflicts between Design and Reality", Bulletin of New Zealand National Society for Earthquake Engineering, Vol. 26, No. 3, pp. 329-341.
71. Priestley, M.J.N. (1995). "Displacement-Based Seismic Assessment of Existing Reinforced Concrete Buildings", Proceedings of 5th Pacific Conference on Earthquake Engineering, Melbourne, Australia, pp. 225-244.
72. Priestley, M.J.N. (1998). "Brief Comments on Elastic Flexibility of Reinforced Concrete Frames and Significance to Seismic Design", Bulletin of New Zealand National Society for Earthquake Engineering, Vol. 31, No. 4, pp. 246-259.
73. Priestley, M.J.N. (2000). "Performance-Based Seismic Design", Proceedings of 12th World Conference on Earthquake Engineering, Auckland, New Zealand, Paper No. 2831.
74. Priestley, M.J.N. and Kowalsky, M.J. (2000). "Direct Displacement-Based Seismic Design of Concrete Buildings", Bulletin of New Zealand National Society for Earthquake Engineering, Vol. 33, No. 4, pp. 421-444.
75. Sadigh, K., Chang, C.Y., Egan, J.A., Makdisi, F. and Youngs, R.R. (1997). "Attenuation Relationships for Shallow Crustal Earthquakes Based on Californian Strong Motion Data", Seismological Research Letters, Vol. 68, No. 1, pp. 180-189.
76. Shibata, A. and Sozen, M. (1976). "Substitute Structure Method for Seismic Design in Reinforced Concrete", Journal of Structural Division, ASCE, Vol. 102, pp. 1-18.
77. Somerville, M., McCue, K. and Sinadinovski, C. (1998). "Response Spectra Recommended for Australia", Australian Structural Engineering Conference, Auckland, New Zealand, pp. 439-444.
78. Toro, G.R., Abrahamson, N.A. and Schneider, J.F. (1997). "Model of Strong Ground Motions from Earthquakes in Central and Eastern North America: Best Estimates and Uncertainties", Seismological Research Letters, Vol. 68, No. 1, pp. 41-57.
79. Venkatesan, S. (2004). "Component Factors for Site Resonance", Departmental Report, Department of Civil and Environmental Engineering, University of Melbourne, Australia.

80. Venkatesan, S., Dhu, T., Lam, N.T.K. and Wilson, J.L. (2003). “The Effect of Rock Motions on Soil Amplification Factors for Australian Conditions”, Proceedings of the Australian Earthquake Engineering Society Annual Conference, Paper No. 16.
81. Watson, S., Zahn, F. and Park, R. (1994). “Confining Reinforcement for Concrete Columns”, Journal of Structural Engineering, ASCE, Vol. 120, No. 6, pp. 1798-1824.
82. Wilkie, J. and Gibson, G. (1995). “Estimation of Seismic Quality Factor Q for Victoria, Australia”, AGSO Journal of Geology and Geophysics, Vol. 15, No. 4, pp. 511-517.
83. Wilson, J.L. and Lam, N.T.K. (2003). “A Recommended Earthquake Response Spectrum Model for Australia”, Australian Journal of Structural Engineering, Institution of Engineers (Australia), Vol. 5, No. 1, pp. 17-27.